Molecular Complexity of Senile Plaques in Alzheimer's Disease

Can it be Modulated by a Targeted Antibody?

Bastrup, Joakim

Publication date:
2019

Document Version
Publisher's PDF, also known as Version of record

MOLECULAR COMPLEXITY OF SENILE PLAQUES IN ALZHEIMER'S DISEASE

CAN IT BE MODULATED BY A TARGETED ANTIBODY?

BY
JOAKIM BASTRUP

DISSERTATION SUBMITTED 2019

AALBORG UNIVERSITY
DENMARK

MOLECULAR COMPLEXITY OF SENILE PLAQUES IN ALZHEIMER'S DISEASE: CAN IT BE MODULATED BY A TARGETED ANTIBODY?

by
Joakim Bastrup, MSc

AALBORG UNIVERSITY
DENMARK

Dissertation submitted
20.12.2019

Dissertation submitted: 20.12.2019

PhD supervisor: Associate Prof. Allan Stensballe,
Aalborg University, Denmark

Assistant PhD supervisors: Dr. Christiane Volbracht,
H. Lundbeck A/S, Denmark

Dr. Ayodeji A. Asuni
H. Lundbeck A/S, Denmark

PhD committee: Clinical Professor Jens Brøndum Frøkjær
Aalborg University

Professor Ole Nørregaard Jensen
SDU Imagine

Associate Professor Ann Brinkmalm
University of Gothenburg

PhD Series: Faculty of Medicine, Aalborg University

Department: Department of Health Science and Technology

ISSN (online): 2246-1302
ISBN (online): 978-87-7210-567-3

Published by:
Aalborg University Press
Langagervej 2
DK – 9220 Aalborg Ø
Phone: +45 99407140
aauf@forlag.aau.dk
forlag.aau.dk

Printed in Denmark by Rosendahls, 2020

PREFACE

The dissertation was submitted as part of the requirements for obtaining a PhD degree at the Doctoral PhD school at Aalborg University, Denmark. The work was conducted as an industrial PhD project in collaboration between Aalborg University, Aalborg, Denmark and the pharmaceutical company H. Lundbeck A/S, Valby, Denmark. The project was partly funded by the Innovation Fund Denmark under file no.: 5189-00044B and was carried out between October 2016 and December 2019. The principal supervisor was Associate professor Allan Stensballe, Department of Health Science and Technology, Aalborg University. The primary and secondary company supervisors were principal scientists Christiane Volbracht and Ayodeji Abdur-Rasheed Asuni, Neuroscience, H. Lundbeck A/S. During the PhD project, a three-month scientific visit was arranged with Dr. Kelly Rogers, Division head; Head, Centre for Dynamic Imaging, Walter and Eliza Hall Institute of Medical Research, Australia.

The main aim of the project was to elucidate the molecular features of senile plaques in Alzheimer's disease and how these are modulated by a target specific antibody. The findings resulted in two publications and one manuscript of which the dissertation is based on:

I. **J. Bastrup,** S. Birkelund, A.A. Asuni, C. Volbracht, A. Stensballe. Dual strategy for reduced signal suppression effects in MALDI mass spectrometry imaging. *Rapid Communications in mass spectrometry*.

II. **J. Bastrup,** K. Kastaniegaard, A.A. Asuni, C. Volbracht, A. Stensballe. Proteomic and unbiased post-translational modification profiling of amyloid plaques and surrounding tissue in a transgenic mouse model of Alzheimer's disease. *Journal of Alzheimer's disease*.

III. **J. Bastrup,** K.H. Hansen, T.B.G. Poulsen, K. Kastaniegaard, A.A. Asuni, S. Christensen, A. Stensballe, C. Volbracht. Anti-Aβ antibody treatment with Aducanumab modified the proteome of senile plaques and surrounding tissue and altered disease progression in a transgenic mouse model of Alzheimer's disease. *Manuscript in preparation*.

[Page left blank intentionally]

ACKNOWLEDGEMENTS

Several people have supported, guided and contributed to the work presented in this PhD dissertation which I am extremely grateful for. The project would not have been possible without this help and I would therefore like to use this section to acknowledge the contributors.

First, I would like to thank the co-founding sources, Aalborg University, H. Lundbeck A/S and the Innovation Fund Denmark, that provided financial support for the project. I would also like to thank my former supervisor, Peter H. Larsen, who came up with the project idea and had a major role in the application and initiation of the project. I appreciate the valuable input and guidance from the co-authors that contributed to the presented publications and manuscript. A big thanks to the people from H. Lundbeck A/S who contributed to the presented work. Thanks to the animal facility, Biologics, the DMPK department and the histology lab (Pia M. Carstensen, Kirsten Jørgensen and Trine Nielsen) for support, input and guidance. I would also like to thank Dr. Kelly Rogers, Dr. Verena Wimmer and the imaging team at the Walter and Eliza Hall Institute of Medical Research for giving the opportunity to visit their imaging department and teaching different techniques. My biggest appreciation goes to my three supervisors who guided me throughout the project. Allan, thank you for providing a mass spectrometry platform that allowed personal development and becoming an independent scientist. Thank you for prioritizing my project and taking the time to participate in skype meetings (even though they were in the middle of the night). Deji, I would like to thank you for your always clever inputs and ideas. I enjoyed and learned from our scientific discussions, particularly our meeting with Professor V. Hugh Perry really encouraged me to continue in this direction. Christiane, a special thanks to you for the always great supervision and your foreseeing skills. I am grateful for the numerous hours we spent on manuscript discussions, writing and adjustments which I learned a lot from. Lastly, I would like to thank my family and friends who have supported me endlessly throughout the project. Especially Freya, thank you for always listening and being there through the ups and downs.

[Page left blank intentionally]

ABBREVIATIONS

ARIA: Amyloid-related imaging abnormalities
1,5-DAN: 1,5-Diaminonaphthalene
2,5-DHA: 2′,5′-dihydroxyacetophenone
3- or 11pE: N-truncated and pyroglutamate modified Aβ
4-HT: 4-Hydroxy-TEMPO
Aβ: Beta-amyloid
Ach: Acetylcholine
AD: Alzheimer's disease
APH1: Anterior pharynx-defective 1
APOE: Apolipoprotein E
APP: Amyloid precursor protein
APS: Ammonium persulfate
BACE1: β-secretase
BIN1: Bridging integrator-1
BSA: Bovine albumin serum
CDR-SB: Clinical Dementia Rating-Sum of Boxes
CHCA: α-cyano-4-hydroxycinnamic acid
CID: Collision-induced dissociation
CLU: Clusterin
CSF: Cerebrospinal fluid
DDA: Data-dependent acquisition
DIA: Data-independent acquisition
DMSO: Dimethyl sulfoxide
EDTA: Ethylenediaminetetraacetic acid
ENO1: Enolase-1
EOAD: Early-onset Alzheimer's disease
ESI: Electrospray ionization
FAD: Familial Alzheimer's disease
FDA: Food and Drug Administration
FFPE: Formalin-fixed, paraffin-embedded
GFAP: Glial fibrillary acidic protein
GWAS: Genome-wide association study
HCD: Higher-energy collisional dissociation
I.p.: Intraperitoneal
I.v.: Intravenous
IgG(1): Immunoglobulin G (subclass 1)
IMS3: Trimodal MALDI-MS imaging
ISD: In-source decay
ITO: Indium-tin oxide
LC-MS/MS: Liquid chromatography tandem-mass spectrometry
LCP1: Plastin-2
LFQ: Label-free quantification
LMD : Laser capture microdissection

LOAD: Late-onset Alzheimer's disease
M/z: Mass-to-charge
MALDI-MS: Matrix-assisted laser desorption/ionization mass spectrometry
MCI: Mild cognitive impairment
MRI: Magnetic resonance imaging
NA: Numerical aperture
NCT: Nicastrin
NFT(s): Neurofibrillary tangle(s)
NMDAr: N-methyl-D-aspartate receptor
NME1: Nucleoside diphosphate kinase A
NS: Normal swine serum
O/N: Over night
Ox: Oxidation
PA: Phosphoric acid
PASEF: Parallel accumulation serial fragmentation
PBS: Phosphate-buffered saline
PCA: Principal component analysis
PEN2: Presenilin enhancer 2
PET: Positron-emission tomography
PFA: Paraformaldehyde
PGK1: Phosphoglycerate kinase 1
PiB: Pittsburgh compound B
PIP5K1C: Phosphatidylinositol 4-phosphate 5-kinase type-1 gamma
ProExM: Protein-retention expansion microscopy
PSEN1/2: Presenilin protein 1 and 2
PTM: Post-translational modification
Pyro-glu: Pyroglutamate
RT: Room temperature
S/N: Signal-to-noise
SA: Sinapinic acid
SAD: Sporadic Alzheimer's disease
SAβPP: Soluble beta-amyloid (Aβ) precursor protein
SDC: Sodium deoxycholate
SDCBP: Syntenin-1
SDHB: Super-2,5-dihydroxybenzoic acid
TEMED: Tetramethylethylenediamine
TFA: Trifluoroacetic acid
Tg: Transgenic
TIC: Total Ion Count (or current)
TIMS: Trapped ion Mobility Spectrometry
TMT: Tandem mass tag
TOF: Time-of-flight
ToF-SIMS: TOF secondary ion mass spectrometry
WD: Working distance

ENGLISH SUMMARY

Alzheimer's disease (AD) is a degenerative brain disease characterized by neuronal loss and progressive accumulation of neurofibrillary tangles and senile plaques. Senile plaques are composed of 38-43 residue beta-amyloid (Aβ) peptides and deposition of these occur in the initial stages of AD. This highlights an association between senile plaques and initiation of biological processes that affect the following pathological events in AD.

We set out to 1) investigate the molecular composition of senile plaques at both a peptide, protein and modification level and 2) investigate whether the molecular composition was affected by a treatment with anti-Aβ targeting antibodies.

We used two optimized tissue-based approaches, matrix-assisted laser desorption-ionization mass spectrometry (MALDI-MS) imaging and a microproteomic approach that combined laser microdissection and liquid chromatography-tandem mass spectrometry (LC-MS/MS). Initial experiments were performed on frozen tissue biopsies from AD brains and from a transgenic (tg) mouse model of AD, the tgAPPPS1-21 mouse model. This mouse model expresses human proteins with mutations causing a hereditary form of AD referred to as familial AD (FAD). Our approaches were used to elucidate whether treatment with the antibody aducanumab could change the proteomic profile of senile plaques in tgAPPPS1-21 mice.

We demonstrated that addition of phosphoric acid (PA) as matrix additive to the super-2,5-dihydroxybenzoic acid (DHB) matrix, significantly improved the signal-to-noise ratio of Aβ1-42 peptides. Our data indicated differences in the peptide composition of Aβ species in senile plaques from AD and tgAPPPS1-21 brains by encompassing more truncated and modified Aβ proteoforms in AD.
Our microproteomic approach identified a total of 555 proteins co-localizing with senile plaques from tgAPPPS1-21 mice. We identified 27 proteins that were significantly regulated by comparing the respective protein levels to adjacent control regions in the tissue. The regulated proteins were associated with cellular processes

such as metabolism and endocytosis. Furthermore, our analysis enabled identification of several exclusive post-translational modifications (PTM) like oxidation, deamidation and pyroglutamylation on proteins co-localizing with senile plaques from the tgAPPPS1-12 mouse brain tissue.

Our chronic treatment with aducanumab reduced the senile plaque load in the hippocampus of tgAPPPS1-21 mice. Using microproteomics, we identified several proteins associated with molecular processes that were modulated by aducanumab. These proteins were associated with metabolism and phagocytosis and were especially regulated in the closely surrounding penumbra of senile plaques.

Our results provide a novel understanding of the complex layers at peptide aggregate, proteome and PTM levels in senile plaques from tgAPPPS1-21 mice. It is considered that these findings can support the development of future treatment strategies targeting senile plaques.

DANSK RESUMÉ

Alzheimers sygdom (AD) er en degenerativ hjernesygdom, der er kendetegnet ved celletab og en gradvis ophobning af neurofibrillære sammenfiltringer samt plak dannelse. Plak indeholder 38-43 lange beta-amyloid (Aβ) peptider og ophobning af plak forekommer i de indledende stadier af AD. Dette indikerer en sammenhæng mellem plak og initiering af biologiske ændringer, der igangsætter den efterfølgende patologi i AD.

Formålet med dette projekt var 1) at undersøge den molekylære sammensætning af plaks, både på et peptid-, protein- og modifikationsniveau og 2) at undersøge om den molekylære sammensætning kunne påvirkes af behandling med antistoffer rettet mod plaks.

Vi benyttede to optimerede vævsbaserede metoder, matrix-assisted laser desorption-ionization mass spectrometry (MALDI-MS) imaging og en mikroprotein analyse, der kombinerede laser dissektion og liquid chromatography-tandem mass spectrometry (LC-MS/MS). I de indledende forsøg anvendte vi frosne vævsbiopsier fra AD hjerner og fra en transgen musemodel for AD, tgAPPPS1-21. Denne musemodel udtrykker humane proteiner med mutationer der medfører en arvelig form af AD, også kaldet familiær AD (FAD). Vores metoder blev anvendt for, at undersøge om behandling med antistoffet aducanumab kunne ændre proteinprofilen af plaks i tgAPPPS1-21 musene.

Vi viste, at brugen af phosphorsyre som matrixadditiv til super-2,5-dihydroxybenzoic acid (DHB) kunne forbedre signal-til-støj-forholdet af Aβ1-42 peptidet signifikant. Vores data indikerede en forskel mellem plak fra AD og tgAPPPS1-21 mus på et peptidniveau, hvor mængden af afkortede og modificerede Aβ former var større i AD. Vores mikroprotein analyse identificerede 555 proteiner, som lokaliserede sig sammen med plak i tgAPPPS1-21 musene. Vi identificerede 27 proteiner, som var signifikant regulerede ved at sammenligne de respektive proteinniveauer til nærliggende kontrol områder i vævet. Disse proteiner var associeret til cellulære

processer som metabolisme og endocytose. Desuden fandt vores analyse eksklusive posttranslationelle modifikationer (PTM) så som oxidering, deamidering og pyroglutamat på proteiner, der lokaliserede sammen med plaks fra hjernevæv fra tgAPPPS1-21 musene.
Vores længerevarende behandling med aducanumab reducerede mængden af plak i hippocampus området i tgAPPPS1-21 musene. Her muliggjorde vores mikroprotein analyse identificering af adskillige proteiner, der var påvirket af aducanumab behandlingen. Disse proteiner var blandt andet associeret til metabolisme og phagocytose og var specielt reguleret i den omkringlæggende plakpenumbra.

Vores resultater giver en ny forståelse af den molekylære kompleksitet, der forekommer på peptid-, protein- og modifikationsniveau i plak hos tgAPPPS1-21 mus. Det vurderes at denne information kan understøtte udviklingen af nye behandlingsstrategier mod plaks.

TABLE OF CONTENTS

[Page left blank intentionally]

CHAPTER 1. BACKGROUND

1.1. ALZHEIMER'S DISEASE (AD): PREVALANCE, CLINICAL SYMPTOMS AND ETIOLOGY

Dementia is characterized by progressive impairment of cognition, function and behavior. It has been estimated that more than 46 million people in the world are currently living with dementia and that the total cost to society was US $818 billion in 2015 (Prince, Wimo, Ali, Wu, & Prina, 2015). Alzheimer's disease (AD) is the most common type of dementia, accounting for approximately 60-70% (World Health Organization, 2017) and is therefore responsible for a large number of dementia cases. Although AD was first described more than hundred years ago, to date, only symptomatic treatments exist which aim to counterbalance the neurotransmitter disturbance and thus no cure exists.

The development of AD can be divided into four stages; preclinical, mild dementia, moderate dementia and severe dementia. At the preclinical stage, daily activities are not significantly affected but mild impairment of planning, ability to acquire new information, accessing general knowledge (semantic memory) and episodic depressive dysphoria may occur. At the mild dementia stage, a notable decrease in learning and memory occurs together with mild impairment of daily activities, language and spatial disorientation (Förstl & Kurz, 1999). At the moderate dementia stage, a significant impairment of daily activity occurs. Patients progressively lose insight into their current disease state and experience incapability of recognizing relatives. The severe dementia stage is characterized by severe memory loss and significant reduction of nearly all cognitive functions. Communication can be reduced to a limited use of words and patients may start to depend on assistance in basic daily activities such as help to chew and swallow while eating (Förstl & Kurz, 1999). It has been estimated that the average time from diagnosis to death is three to nine years, strongly associated with the age at diagnosis (Brookmeyer, Corrada, Curriero, & Kawas, 2002). A variety of environmental and genetic factors have been associated with AD. The disease is characterized as either familial early onset (EOAD; FAD) or

sporadic late-onset (LOAD; SAD). Autosomal-dominant mutations in the amyloid precursor protein (*APP*), Presenilin 1 (*PSEN1*) and Presenilin 2 (*PSEN2*) genes are associated with EOAD (Chartier-Harlin et al., 1991; Rogaev et al., 1995; Sherrington et al., 1996). The genetic factors involved in SAD are complicated in that genome-wide association studies (GWAS) have identified several potential loci (at least 29 loci) that increases the risk of developing SAD (Jansen et al., 2019; Lambert et al., 2013). These single-nucleotide variants are observed in genes such as apolipoprotein E (*APOE*), clusterin (*CLU*), and bridging integrator 1 (*BIN1*).

1.2. NEUROPATHOLOGICAL HALLMARKS OF AD

1.2.1. MACRO- AND MICROSCOPIC CHARACTERISTICS

Macroscopic examination of an AD brain reveals a characteristic pattern of brain dystrophy. This appears particularly as cortical atrophy and thinning, and dilation of the lateral ventricles (**Figure 1-1A**; (Serrano-Pozo, Frosch, Masliah, & Hyman, 2011)). At a microscopic level, positive and negative lesions can be observed. The positive lesions include: 1) extracellular senile plaques (also referred to as amyloid plaques) that are mainly composed of 38-43 residue beta-amyloid peptides (Aβ; **Figure 1-1B**). 2) Neurofibrillary tangles (NFTs) and neuropil threads, which are both intracellular inclusions made of aggregated and hyperphosphorylated tau (**Figure 1-1C**) and 3) dystrophic neurons. The negative lesions include loss of neurons, neuropil regions and synaptic elements (Serrano-Pozo et al., 2011).

Longitudinal studies assessing cognitive evaluation together with biomarkers in cerebrospinal fluid (CSF) and advanced imaging techniques such as positron emission tomography (PET) imaging have identified a preclinical phase in AD occurring 10-20 years before clinical symptoms initiates (Jack et al., 2010). The PET studies have for example used an amyloid PET ligand (Pittsburgh compound B (PiB)) to measure the amyloid deposition (Klunk et al., 2004). In this prodromal phase, changes in Aβ accumulation and subsequently NFTs have been identified, highlighting the pathological relevance of these hallmarks in the initial phase of AD (Jack et al., 2010) (**Figure 1-1D**).

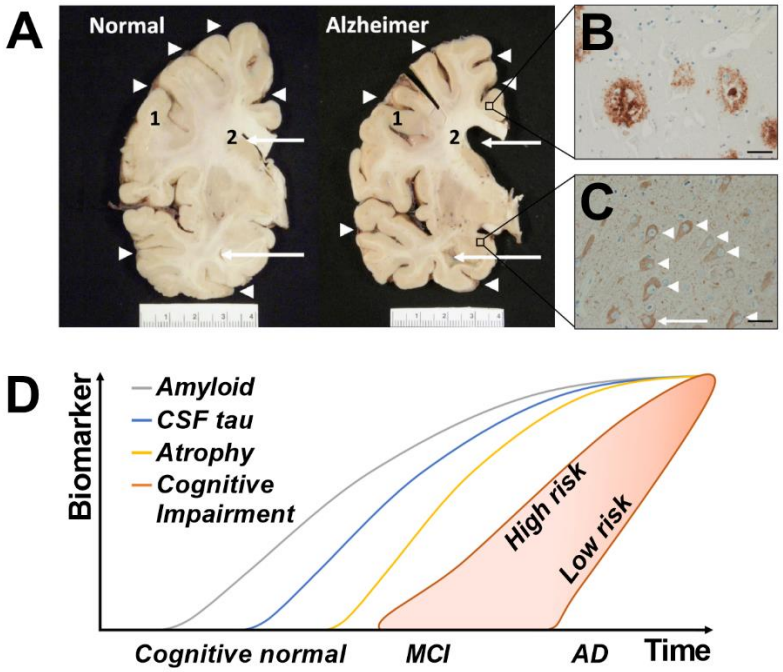

Figure 1-1: A) Anatomical comparison of healthy brain and Alzheimer's disease (AD) brain. Shrinkage of the cerebral cortex (1) accompanied by enlarged ventricles (2) is detectable at a macroscopic level in AD (right). Senile plaques (B) and neurofibrillary tangles (C) are detectable at a microscopic level. Scale bar = 40 µm. D) Hypothetical modeling of AD trajectory. By using different techniques, the presence and progression of different biomarkers, beta-amyloid (Aβ), CSF tau, atrophy by magnetic resonance imaging (MRI) and cognitive impairment, can be outlined. Positron emission tomography (PET) can be used to observe radioactive tracers like the Pittsburgh compound B (PiB; grey) that is a radioactive analog to the amyloid-binding compound thioflavin-T. These changes are thought to initiate the tau-associated pathology which causes release of the tau protein from dying neurons that can be detected in the cerebrospinal fluid (CSF; blue). The tau-associated pathology is followed by brain atrophy measured by MRI (yellow). Mild cognitive impairment (MCI) and symptoms of AD will occur over time. Genetic factors can

affect the presence of these biomarkers and thereby affect the progression of the disease. Figure 1A-C was modified from (DeTure & Dickson, 2019) with permission from the copyright owner (Springer Nature; under terms of the Creative Commons Attribution 4.0 International License[1]. Figure 1D was made by Joakim Bastrup and modified from (Fan, Brooks, Okello, & Edison, 2017; Jack et al., 2010).

Amyloid-β peptides, aggregation and senile plaque deposition

Several hypotheses have been formulated to explain mechanisms leading to AD pathogenesis. The widely accepted "amyloid cascade hypothesis" states that a chronic imbalance between the production and clearance of Aβ peptides leads to increased levels and deposition of Aβ peptides in the prodromal phase of AD (Hardy & Selkoe, 2002; Masters, Simms, Weinman, Multhaupt, & Mcdonald, 1985). The Aβ peptide is derived from the integral membrane APP in a sequential cleavage process by two enzymes. First, beta (β)-secretase (BACE1) cleaves APP at the N-terminal of Aβ, resulting in a membrane-anchored C-terminal fragment of AβPP and release of a soluble APP fragment (**Figure 1-2**). Second, the anchored AβPP fragment is cleaved by gamma (γ)-secretase complex, consisting of PSEN1 or PSEN2, anterior pharynx-defective 1 (APH1), nicastrin (NCT) and presenilin enhancer 2 (PEN2) (reviewed by (Annaert & De Strooper, 2002); **Figure 1-2**).

The C-terminal cleavage by γ-secretase can vary and therefore result in generation of different variants of Aβ such as Aβ1-38, Aβ1-40, Aβ1-42, Aβ1-43. The anchored AβPP can also be cleaved by alpha (α)-secretases that results in sAPPα. This variant (sAPPα) has been reported to have neuroprotective functions and cleavage through this pathway is considered the non-amyloidogenic pathway (Furukawa et al., 2002).

The Aβ peptide contains both hydrophilic and hydrophobic domains which is explained by the extracellular and transmembranal location of APP. However, these features also cause different aggregation properties of Aβ peptides, depending on the

[1] http://creativecommons.org/licenses/by/4.0/

length of the peptides (Barrow & Zagorski, 1991). The induced aggregation properties cause formation of oligomers, fibrils and eventually extracellular senile plaques.

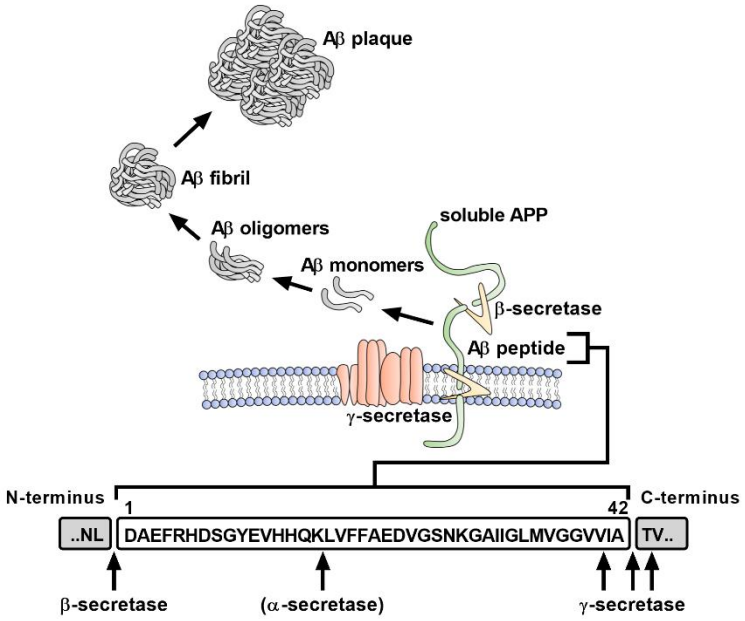

Figure 1-2: Graphical illustration of beta-amyloid (Aβ) sequence and processing from amyloid precursor protein (APP) to senile plaque (Aβ plaque). The transmembrane APP is cleaved by β-secretase and γ-secretase, leading to generation of an Aβ monomer. Aβ monomers can aggregate into oligomers (and protofibrils), Aβ fibrils and Aβ plaques. The different cleavage sites by secretases are illustrated by the arrows. The figure was modified from (Panza, Lozupone, Logroscino, & Imbimbo, 2019) and made by Joakim Bastrup.

Senile plaques are generally divided into two types, diffuse and neuritic plaques (also called dystrophic plaques). Diffuse plaques are deposited in a non-fibrillar conformation whereas the neuritic plaques are deposited in a fibrillar confirmation (Probst, Brunnschweiler, Lautenschlager, & Ulrich, 1987). Neuritic plaques are associated with surrounding degenerated neurites. Several studies have reported glial cell engagement of senile plaques, indicating that plaques are in close contact with the surrounding environment (Akiyama et al., 1999; Heneka et al., 2015). Furthermore,

proteins such as APOE, CLU and BIN1, have been reported to co-localize with aggregated Aβ, either directly or in close contact (De Rossi et al., 2019; Koistinaho et al., 2004; Oda et al., 1995). For example, APOE has been hypothesized to affect Aβ aggregation and clearance, whereas CLU has been reported to generate oxidative stress upon co-aggregating with Aβ (Koistinaho et al., 2004; Oda et al., 1995). BIN1 on the other hand, has been reported to localize at a pathogenic region within periphery regions of senile plaques and thus not in direct aggregation with the entire unit of the plaque (De Rossi et al., 2019). These examples suggest a pathological relevance for some of the co-localizing proteins, as they can impact aggregation, clearance and spreading of Aβ (reviewed by (Atwood, Martins, Smith, & Perry, 2002)) (**Figure 1-3**).

Several reports have shown that Aβ aggregates mainly exist as truncated isoforms rather than full length Aβ peptides (Güntert, Döbeli, & Bohrmann, 2006; Liu et al., 2006; Piccini et al., 2005). Among these, pyroglutamate (pyro-glu) modified Aβ isoforms are a predominant component observed in senile plaques in AD patients (Jawhar, Wirths, & Bayer, 2011; Moro et al., 2018). It has been suggested that pyro-glu modified Aβ peptides accumulate in the brain at the earliest stages, before the appearance of clinical symptoms of AD, indicating that these peptides could potential be seeding species and thus play an important role in the subsequent aggregate formation (Sergeant et al., 2003). Pyro-glu modified Aβ is generated in a two-step process by first an N-terminal truncation at a glutamate residue followed by processing of glutaminyl cyclase that catalyze the generation of cyclic pyroglutamate (Jawhar et al., 2011). Despite the relevance of the pyro-glu modifications, Aβ peptides have also been reported to contain other post-translational modifications (PTMs) like racemization, isomerization, phosphorylation, nitration, dityrosine, glycosylation and oxidation (reviewed by (Kummer & Heneka, 2014)). One explanation for this variety of PTMs could be the extracellular location of aggregated Aβ peptides in which they are exposed to an extracellular environment and/or secreted enzymes (reviewed by (Atwood et al., 2002)). Additionally, given that several proteins infiltrate and interact with senile plaques, it is unknown whether such exposure is affecting the co-localizing

proteins. PTMs have been reported to change the confirmation and biological function of proteins (Jensen, 2004) and exposure to PTMs could therefore have significant impact on the biological processes occurring within and around senile plaques (e.g. affect the aggregation, clearance rate and/or seeding in a both beneficial or detrimental way (**Figure 1-3**)).

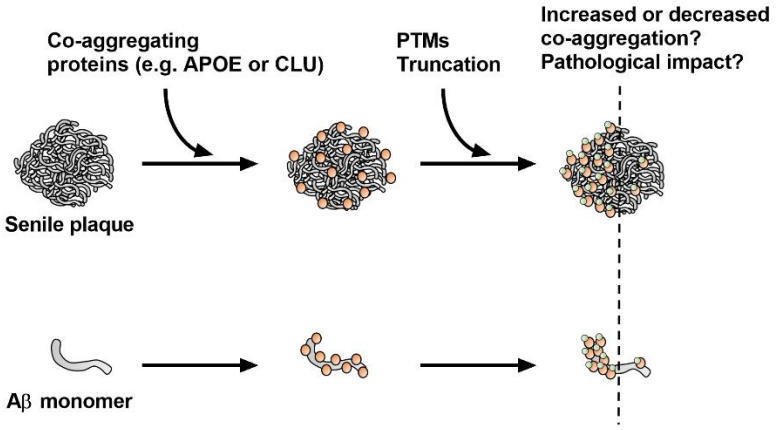

Figure 1-3: Hypothetical illustration of proteins co-aggregating with beta-amyloid (Aβ). Proteins such as apolipoprotein E (APOE) and clusterin (CLU) have been reported to co-aggregate directly with Aβ and affect clearance, toxicity and deposition. Several post-translational modifications (PTMs) and truncation variants have been identified on Aβ, but it is unknown whether co-aggregating proteins are 1) also subjected to such modifications and/or 2) are affected by PTMs or truncation of Aβ. Figure was made by Joakim Bastrup.

Tau, NFT formation and relation to amyloid-β

NFTs represent the second major hallmark of AD and arises from intraneuronal aggregates of the microtubule-associated protein tau. Tau is encoded by the *MAPT* gene and functions as a stabilizing phosphoprotein that contributes to the assembly and structure of axonal microtubules and neuronal transport (reviewed by (Zempel & Mandelkow, 2014)). The human tau protein can be spliced into six isoforms that are differentially expressed throughout the development of the brain (Goedert, Spillantini, Potier, Ulrich, & Crowther, 1989). Under pathological conditions tau can undergo

multiple PTMs such as hyperphosphorylation, further mis-localization, oligomerization, and aggregation events. Tau aggregation can lead to several forms such as paired helical filaments, twisted ribbons and straight filaments that consequently form NFTs in AD (Goedert, Spillantini, Cairns, & Crowther, 1992; Goedert, Spillantini, & Crowther, 1991). The formation and spreading of NFTs in the brain of AD patients is believed to disrupt normal tau function and result in synapse loss, neuronal death and cognitive impairment. The appearance of NFTs in different brain regions is classified into stages of AD (Braak & Braak, 1991). Importantly, the level of NFTs in the neocortex correlates with the cognitive decline in AD which is different from the Aβ-associated pathology (Nelson, Braak, & Markesbery, 2009). Recent reports suggest that the tau-associated pathology propagates throughout the AD brain via neuronal circuits in a prion like manner (reviewed by (Zempel & Mandelkow, 2014)).

The relationship between Aβ accumulation and subsequent initiation of tau pathologies has long been debated. It has been found that Aβ dimers extracted from AD brains increase hyperphosphorylation of tau as well as neurodegeneration in a neuronal cell culture (Jin et al., 2011). Similarly, a recent study developed a three-dimensional human stem-cell-derived culture system expressing FAD mutations, and observed hyperphosphorylated tau and tau aggregates after Aβ deposition (Choi et al., 2014). Although these studies are not comprehensive, they indicate a link between Aβ and the tau-associated pathology.

1.3. MOUSE MODELS MIMICKING THE AMYLOID-ASSOCIATED PATHOLOGY

Transgenic (tg) mouse models have been generated to mimic core features of AD pathology such as Aβ accumulation and deposition. The design of several tg amyloid-models is based on FAD mutations like the autosomal dominant mutations in the *APP*, *PSEN1*, or *PSEN2* genes. These FAD mutations account for approximately 1% of all AD cases, with an established probability of 50% for developing AD when inherited one of the three mutations (reviewed by (Bateman et al., 2010)). The human and mouse APP share 97% sequence homology. Notably, the mouse Aβ sequence contains

three different amino acids compared to the human homolog (R5G, Y10F, H12R) that hinders Aβ overproduction and aggregation in mice (Xu et al., 2015). Thus, cloning the human FAD mutated *APP* gene into mice has been found necessary to model the excessive generation of Aβ seen in FAD patients. Overexpression of human APP without FAD mutations did not result in deposition of senile plaques mice (Mucke et al., 2000). Several models carrying different designs have been developed. The most common examples are the tg2576, tgAPP$_{ArcSwe}$ and tgAPP23 models overexpressing human APP isoforms (APP695 or APP751) containing the double Swedish mutation (KM670/671NL) or the Swedish mutation in combination with the Artic mutation (E693G) (Hsiao et al., 1996; Lord et al., 2006; Sturchler-Pierrat et al., 1997). Similarly, the tgAPPPS1-21 and tgPS2APP models have been generated to overexpress human APP with the Swedish mutation while also carrying either mutated human PSEN1 (L166P) or PSEN2 (N141I) (Radde et al., 2006; Richards et al., 2003). In general, these tg mice develop a robust senile plaque deposition throughout the brain and feature signs of gliosis that is observed in AD. However, these models show limited hyperphosphorylated tau and have not been reported to develop NFTs (reviewed by (Drummond & Wisniewski, 2017)). Additionally, global neuron loss (e.g. brain atropy) is also limited in these FAD models (Takeuchi et al., 2000). Therefore, these models do not recapitulate FAD, but rather mimic overproduction of Aβ and how the mouse brain environment copes with such accumulation. These models are widely used to support the development of new drugs targeting Aβ and it is considered important to investigate the translatability between these models, FAD and AD.

1.4. TREATMENT STRATEGIES TARGETING AMYLOID-B

Currently, only symptomatic treatments for AD are available. These drugs are cholinesterase inhibitors and a N-methyl-D-aspartate receptor (NMDAr) antagonist that increase levels of acetylcholine (ACh) or block stimulation of the NMDAr, respectively (reviewed by (Godyń, Jończyk, Panek, & Malawska, 2016)). As these symptomatic treatments do not halt or delay the disease progression, there is an unmet need for finding new treatments. Therefore, disease-modifying drugs that can interfere

with the pathological steps leading to clinical symptoms, are currently of high interest and under extensive research. The amyloid cascade hypothesis postulates that several steps are involved in Aβ release, processing and formation of senile plaques (**Figure 1-2**). These different stages contain promising targets because of the strong involvement of Aβ in the prodromal phase of AD. For example, the processing of APP involves secretases (BACE1 and γ-secretase) that can be inhibited. The aggregation process of monomers into oligomers, protofibrils and Aβ fibrils can also be inhibited, stopped or directed into increased degeneration by aggregation inhibitors. Further, the aggregation process from Aβ fibrils into senile plaques can be inhibited and targeted for increased clearance by anti-Aβ antibodies (reviewed by (Panza et al., 2019); **Figure 1-4**).

Anti-Aβ immunotherapies aiming at increasing the clearance of Aβ species and senile plaques are currently one of the promising treatment concepts that enter phase III clinical trials. These include active or passive immunization strategies. Active immunization uses exposure to an Aβ antigen that triggers an immunological response that provokes the generation of antibodies against an Aβ epitope. One example of an active vaccine was AN-1792 that greatly reduced senile plaque burden, but introduced aseptic meningoencephalitis in few patients in a phase II trial (Nicoll et al., 2003; Schenk et al., 1999). The benefits of active vaccinations are the extended antibody response of polyclonal antibodies that limit the number of vaccinations while targeting multiple sites. On the other hand, a risk of producing adverse effects is present which was observed in the AN-1792 trial (Nicoll et al., 2003).

The passive immunization strategies include administration of monoclonal or polyclonal antibodies that target different steps in the APP processing and senile plaque formation (**Figure 1-4**). Several antibodies such as bapineuzumab, solanezumab, gantenerumab, crenezumab and aducanumab have entered clinical trials but failed to reach the primary endpoints (reviewed by (Selkoe, 2019; van Dyck, 2018)). Different hypotheses have been proposed for how clearance mechanisms are facilitated by the anti-Aβ immunotherapies. For example, the peripheral sink hypothesis postulates that antibodies facilitate the transport of Aβ peptides across the

blood-brain barrier into periphery by thriving towards creating an equilibrium between the brain and periphery (Zhang & Lee, 2011). In contrast, a central clearance mechanism has also been proposed where the degradation is mediated by glial cell engagement and/or antibody binding and inhibition of further aggregation or spreading of toxic oligomers (Bohrmann & Baumann, 2012; Sevigny et al., 2016).

Two antibodies, gantenerumab and aducanumab, were of interest in this PhD thesis because they have shown promising results in preclinical animal models while having different target profiles and are investigated in clinical trials. A short introduction to both antibodies will be given in the following section.

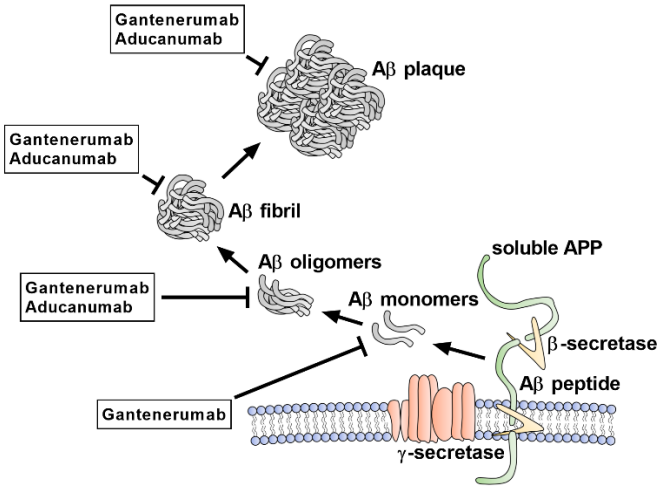

Figure 1-4: Graphical illustration of beta-amyloid (Aβ) processing as illustrated previously in (**Figure 1-2)**. Each step can be targeted by different antibodies like gantenerumab and aducanumab. Figure was modified from (Panza et al., 2019) and made by Joakim Bastrup.

1.4.1. TWO ANTIBODIES OF INTEREST, GANTENERUMAB AND ADUCANUMAB

Gantenerumab or RG1450, is a human immunoglobulin G subclass 1 (IgG1) monoclonal antibody by Hoffman-La Roche with high binding affinity against a

conformational epitope on Aβ that includes both the N-terminal and mid region of Aβ peptides (sequence: AA 3-12 and AA18-27) (Bohrmann & Baumann, 2012). The antibody is hypothesized to recruit microglia and increase phagocytosis of aggregated Aβ. The initial phase I clinical trials showed removal of senile plaques measured by Aβ PET imaging (Ostrowitzki et al., 2012), although amyloid-related imaging abnormalities (ARIA) were of concern (e.g. vasogenic edema). Two phase III clinical trials, called GRADUATE 1 and 2 in early (prodromal to mild) AD patients, are currently ongoing.

Aducanumab or BIIB037, is a human IgG1 monoclonal antibody by Biogen with high binding affinity against oligomeric and insoluble fibrillar Aβ1-42 (sequence: AA3-6) (Sevigny et al., 2016). Results from the initial phase I trial with a small cohort (n = 165 patients) was very promising and showed significant clearance of senile plaques, visualized by Aβ PET imaging, and decelerating of cognitive decline measured by Clinical Dementia Rating-Sum of Boxes (CDR-SB) (Sevigny et al., 2016). Based on these positive findings, two phase III trials (Emerge and Engage) with larger cohorts of mild AD patients (n = 3200 combined) were conducted and showed efficient removal of senile plaques by PET imaging (reviewed by (Selkoe, 2019)). However, in the first analysis cognition measured by CDR-SB was not improved in patients receiving aducanumab, and thus the trials were terminated in spring 2019. The negative outcome of these aducanumab trials led to several questions around why cognitive decline was not slowed when Aβ deposition was efficiently removed as well as to the relevance of the amyloid cascade hypothesis in AD. Other points such as trial design, inclusion of patients with advanced Aβ pathology, or reliability of PET imaging have also been questioned (reviewed by (Selkoe, 2019)). However, in October 2019, based on a new analysis of a larger dataset from the discontinued studies, it was reported that aducanumab reduced patients' clinical decline measured by CDR-SB significantly in the high-dose aducanumab group of the Emerge trial. Approval of aducanumab by the Food and Drug Administration (FDA) based on a single positive trial is pending.

These recent developments highlighted all the complexity of targeting Aβ in AD. It is also a reminder that we need a much better understanding of the underlying biology, as well as molecular markers that link to the disease and the prodromal phase of AD. Furthermore, we need tools that can elucidate the molecular effects of treatments that are in development.

1.5. TISSUE-BASED APPROACHES TO INVESTIGATE THE COMPOSITION OF SENILE PLAQUES

The amyloid cascade hypothesis postulates that excessive production and accumulation of Aβ over time leads to formation of senile plaques and subsequently triggers pathological and detrimental changes in brain function. Therefore, characterizing senile plaques within the tissue-associated environment is key to understanding the cellular and immunological interaction and subsequent pathological cascade of events in AD. Several technologies are available to elucidate this, but we reasoned that unbiased and hypothesis-free techniques such as RNA-sequencing or mass spectrometry are advantageous approaches because of their broad identification capabilities. Two mass spectrometry-based strategies have been used in the course of this PhD project and a general introduction and their previous applicability in relation to AD will be described in the subsequent sections.

1.5.1. MALDI-MS IMAGING ANALYSIS OF SENILE PLAQUES

Introduction to MALDI-MS

Matrix-assisted laser desorption/ionization mass spectrometry (MALDI-MS) was introduced in the mid 1980's by discovering the capability of ionizing molecules by laser ablation in combination with UV light absorbing matrix compounds (Karas, Bachmann, & Hillenkamp, 1985; Karas & Hillenkamp, 1988; Tanaka et al., 1988). The fundamental principles of MALDI-MS are also applicable to MALDI imaging and a short introduction to MALDI-MS will therefore be described in this section.

In MALDI-MS, a sample such as a peptide or protein mixture is mixed with a solution containing a sample matrix, usually an organic molecule having specific characteristics that enables its usability. The most important feature of the matrix is

to adsorb energy and facilitate ionization of the sample compound during irradiation by a laser beam without causing radiational damage to the specimen. Such high energy density within the matrix lattice results in a phase transition of the molecules from solid state into gas phase ions. Notably, this is a soft ionization with little increase in internal energy, meaning that little to no fragmentation occurs when analyzing molecules and thus ionized molecules are generally intact (Tanaka et al., 1988). After ionization, molecular ions can be detected by a mass analyzer and detector that determines the *mass-to-charge* (m/z) ratio of the ions. This is commonly based on a time-of-flight (TOF) measurement where the analytes are accelerated by an electric field and guided into a TOF mass analyzer (Tanaka et al., 1988). The electric field is uniform and applies the same amount of energy to all ions, meaning that the travel through the TOF mass analyzer is dependent on the m/z ratio of the ions. The information from this measurement can be presented as a mass spectrum depicting the intensity (number of ions) as a function of the m/z value.

Commonly employed matrices for peptide and protein analysis are sinapinic acid (SA; (Ronald C. Beavis, Chait, & Standing, 1989)), α-cyano-4-hydroxycinnamic acid (CHCA; (R. C. Beavis, Chaudhary, & Chait, 1992)) and 2,5-dihydroxybenzoic acid (2,5-DHB; (Strupat, Karas, & Hillenkamp, 1991). The choice of matrix depends on the target molecule of interest as the matrix' ability to adsorb/desorb and ionize different classes of molecules vary. The matrix compounds are commonly in a combination with an organic solvent (e.g. acetonitrile or methanol) and an organic acid (e.g. trifluoroacetic acid (TFA) or formic acid) that affect crystal morphology, reproducibility and signal-to-noise (S/N) ratio (Laugesen & Roepstorff, 2003). Different organic acids have been investigated to improve the matrix capabilities by enhancing sensitivity and reducing signal suppression effects. For example, phosphoric acid (PA) has been observed to enhance the detection of phosphopeptides and non-phosphopeptides in combination with the 2,5-DHB matrix (Kjellstrtöm & Jensen, 2004; Kuyama, Sonomura, & Nishimura, 2008; Park, Kim, Lee, Seo, & Kim, 2013; Stensballe & Jensen, 2004).

Introduction to MALDI-MS imaging

In 1997, Caprioli and colleagues showed that the spatial distribution of molecules could be mapped on sections from rat pituitary tissue by using MALDI-MS directly on the tissue, thereby introducing MALDI-MS imaging (Caprioli, Farmer, & Gile, 1997). By taking advantage of MALDI-MS principles, MALDI imaging enables detection, identification and spatial distribution of a variety of different molecules. MALDI-MS imaging data is acquired by ablating the surface of a sample by a series of spots covering an area of interest by a predefined number of laser shots per x,y coordinate (reviewed by (Norris & Caprioli, 2013)). Each spot contains mass spectral data that together is used to generate a plot of ion intensities (single ion images) and enable visualization of molecules within the analyzed sample specimen at relative high resolution (**Figure 1-5**). Sample preparation steps such as handling, pretreatment, matrix type and deposition are important features in MALDI-MS imaging that affects morphological detail, analyte sensitivity and spatial resolution. For example, fresh frozen tissue cut at 3-20 µm thickness and mounted on conductive glass slides (indium-tin oxide (ITO)) are typically preferred to ensure an electrical conductance between tissue section and glass slide. Proper rinsing or washing of the tissue specimen is critical for removing signal suppressing molecules like salts and lipids that may affect crystallization or cause adduct formation (reviewed by (Norris & Caprioli, 2013)). Several washing steps are typically used when analyzing peptides or proteins in tissue to effectively reduce the interference of salts and lipids. One of these include a combination of ethanol and Carnoy's fluid (chloroform, acetic acid and ethanol) (Yang & Caprioli, 2011). The choice of matrix compound, organic solvent, additive and matrix deposition method can affect the outcome of the analysis. Each type of matrix has advantages and disadvantages and thus identifying the optimal matrix is often depending on the tissue type and molecule species of interest (e.g. lipid or peptide (Kaya, Zetterberg, Blennow, & Hanrieder, 2018)). Several commercially available matrix deposition instruments exist such as the ImagePrep (Bruker Daltonics) and the TM-sprayer (HTX Technologies). One advantage with these robotic sprayers compared to manual deposition or sublimation is the possibility of adjusting the deposition settings (e.g. dry time; matrix wetness, microcrystal structure,

and layer thickness) and thereby designing the optimal matrix deposition for a given tissue sample and the applied matrix. Any changes in the deposition parameters will potentially introduce matrix variability between experiments.

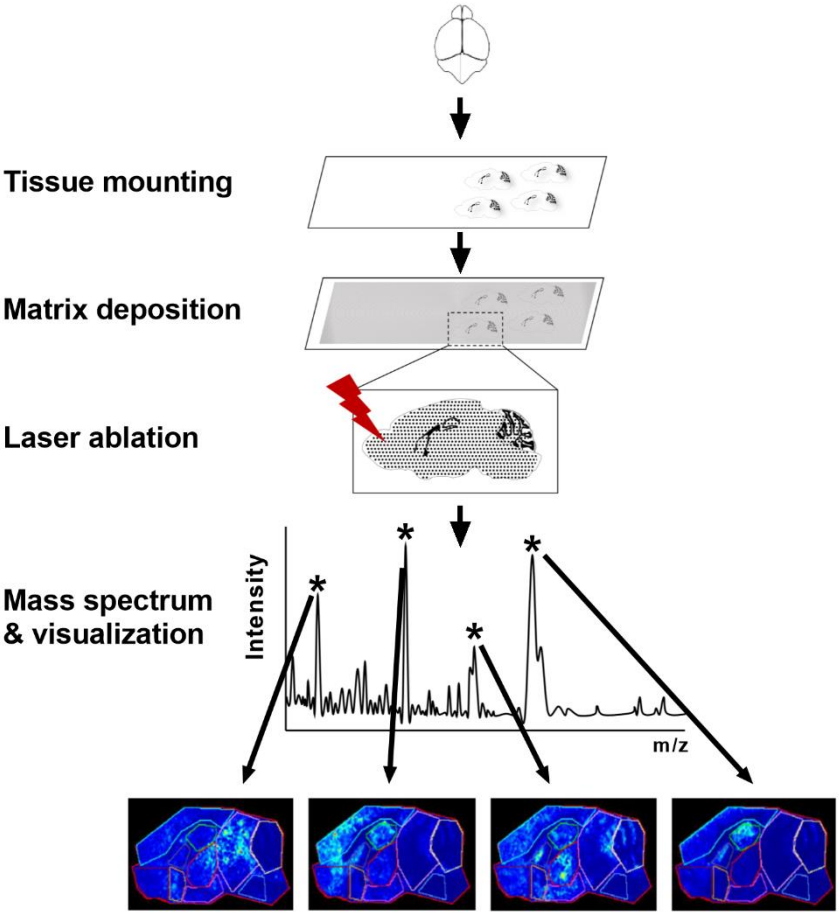

Figure 1-5: Matrix assisted laser desorption/ionization mass spectrometry (MALDI-MS) imaging workflow. A sample specimen (here mouse brain) is sectioned and mounted to a conductive glass slide. An organic matrix solution is applied, and a series of spots are ablated with a laser beam. A mass spectrometer is used to detect the generated ions and create a mass spectrum for each spot. By combining mass spectral data from all spots single ion-images can be generated and used to visualize the spatial distribution of molecules of interest. Figure was made by Joakim Bastrup.

MALDI-MS imaging of senile plaques

MALDI-MS imaging is reasoned to be advantageous for elucidating the senile plaque location and composition in tissues because it does not require multiple immunostainings. The use of MALDI-MS imaging to study Aβ peptides and aggregates have emerged over the last years (**Table 1-1**). Initially, Stoeckli and colleagues reported a method for spatial detection of Aβ peptides in brain tissue sections from tgAPP23 mice in 2002 (Stoeckli, Staab, Staufenbiel, Wiederhold, & Signor, 2002). The tissue sections were mounted on stainless-steel sample plates and the SA matrix was manually applied. This approach led to the detection of Aβ1-37, Aβ1-38, Aβ1-39, Aβ1-40, Aβ1-42 and Aβ1-42 Oxidized form (Ox) using the Voyager STR mass spectrometer (Applied Biosystems) (Stoeckli et al., 2002). Using a thin-layer chromatography sprayer, Stoeckli and colleagues also showed the first fragmentation spectrum of Aβ1-42 on tissue using the CHCA matrix (Stoeckli et al., 2006). In 2008, Seeley and colleagues reported similar ability to detect senile plaques by MALDI-MS imaging using several matrices (Seeley & Caprioli, 2008). In 2016, Kelley and colleagues reported a method for detecting Aβ peptides by laser-induced in-source decay (ISD) combined with MALDI-MS imaging with the purpose of avoiding subsequent conformational MS/MS analysis that was reported to be difficult in formalin-fixed, paraffin-embedded (FFPE) tissue (Kelley, Perry, Castellani, & Bach, 2016). Kelley and colleagues compared mass spectra from synthetic Aβ and isolated senile plaque material from FFPE AD brain and identified Aβ peptide fragments ((Kelley, Perry, Bethea, Castellani, & Bach, 2016; Kelley, Perry, Castellani, et al., 2016)). This approach enabled detection of several Aβ species (Aβ1-16, Aβ1-24, Aβ5-40, Aβ14-40, Aβ1-42). Notably, a trypsin digest step was found necessary to detect Aβ species (Kelley, Perry, Castellani, et al., 2016). In contrast to the previous approaches, the brain tissue was mounted onto ITO conductive glass slides and on-tissue trypsin digest was performed prior to sublimation with the 2,5-DHB matrix. Moreover, the analysis was acquired on a Ultraflextreme instrument (Bruker Daltonics) (Kelley, Perry, Bethea, et al., 2016; Kelley, Perry, Castellani, et al., 2016).

In 2016, Carlred and colleagues used MALDI-MS imaging on brain sections from a model carrying the Artic and Swedish mutation in AβPP ($tgAPP_{ArcSwe}$). Additionally, they used laser capture microdissection (LMD) and MALDI-MS to validate the mass of different Aβ peptides detected in the MALDI-MS imaging analysis (Carlred et al., 2016). Their setup included fresh frozen tissue and the CHCA matrix that was applied with the ImagePrep sprayer. The analysis was performed on a Ultraflextreme instrument model (Carlred et al., 2016). The study detected several Aβ species without tryptic digest, including: Aβ1-42arc Ox, Aβ1-42arc, Aβ1-42arc Ox $[M+2H]^{2+}$, Aβ1-40arc $[M+Na]^{+}$, Aβ1-40arc, Aβ4-43arc Ox, pyro-glu modified Aβ3-42, Aβ1-39arc, Aβ2-40arc, Aβ5-43 Ox, Aβ3-40arc $[M+Na]^{+}$, Aβ3-40arc Ox, Aβ1-38arc $[M+Na]^{+}$, Aβ1-38arc Ox, Aβ1-38arc, Aβ2-39arc, Aβ1-37arc, Aβ3-39arc Ox, Aβ1-36arc, Aβ11-40arc, Aβ7-28arc, Aβ11-33arc.

In 2016, Mendis and colleagues reported detection of lipid changes in AD brain compared to healthy control (Mendis, Grey, Faull, & Curtis, 2016). The study used sublimation with the 1,5-Diaminonaphthalene (1,5-DAN) matrix and analyzed the tissue specimens with the Ultraflextreme instrument. Both negative- and positive-ion modes were used on adjacent tissue sections to investigate lipids changes in the hippocampus (Mendis et al., 2016). In 2017, Kaya and colleagues similarly studied lipid changes in the $tgAPP_{ArcSwe}$ mouse model of AD (Kaya, Brinet, Michno, Syvänen, et al., 2017). The study focused on detecting gangliosides and ceramides species using a similar experimental setup as reported by Mendies and colleagues (2016) (e.g. 1,5-DAN matrix, sublimation, Ultraflextreme analysis in negative-ion mode (Kaya, Brinet, Michno, Syvänen, et al., 2017)). Kaya and colleagues did not detect senile plaques with MALDI-MS imaging but correlated the MALDI-MS imaging data with histological staining of senile plaques (Kaya, Brinet, Michno, Syvänen, et al., 2017; Kaya, Michno, et al., 2017). The same year, the group published a three-step method termed trimodal MALDI-MS imaging (IMS3) to study lipids and peptides within the same tissue section (Kaya, Brinet, Michno, Zetterberg, & Blenow, 2017). With IMS3, a dual polarity (both negative and positive-ion mode) was used on the same spot with 1,5-DAN matrix followed by an additional analysis using a second matrix, 2′,5′-

dihydroxyacetophenone (2,5-DHA), for peptide imaging on the Ultraflextreme instrument (Kaya, Brinet, Michno, Zetterberg, et al., 2017). By including the second matrix, the authors were able to detect Aβ1-37, Aβ1-38 and Aβ1-40 and correlate changes of lipids (sphingolipids, phospholipids and lysophospholipids) with senile plaques in the tgAPP$_{ArcSwe}$ mouse model of AD (Kaya et al., 2018). The IMS3 approach has further been optimized by including LMD and immunoprecipitation in combination with MALDI-MS to elucidate lipid changes in AD (Michno et al., 2018). Moreover, recent combinations with multimodal TOF secondary ion mass spectrometry (ToF-SIMS) and multivariate image analysis have indicated lipid associated differences across senile plaques in brain tissue from tgArcSwe mice (Michno, Wehrli, Zetterberg, Blennow, & Hanrieder, 2019).

In 2017, Kakuda and colleagues analyzed AD patient tissue with MALDI-MS imaging to visualize the spatial distribution pattern of Aβ peptides (Kakuda, Miyasaka, Iwasaki, Nirasawa, & Wada-kakuda, 2017). By using the SA matrix and one of three methods for matrix deposition (airbrush, ultrasonic sprayer or automatic sprayer) and the Rapiflex instrument (Bruker Daltonics). This enabled identification of a distinct distribution pattern of senile plaques in AD brain tissue that was associated with Aβ peptide variants (Kakuda et al., 2017). The study used formic acid (vapor) pretreatment that was reported to improve detection of Aβ peptides. The study was the first to report detection of pyro-glu modified Aβ species in human AD brain tissue using MALDI-MS imaging. In addition to the pyro-glu modified Aβ, they also detected a variety of different Aβ species, such as Aβx-40 and Aβx-42 (x = 2, 4, 5, 6, 7, 8, 9 and 10) (Ikegawa et al., 2019; Kakuda et al., 2017) (**Table 1-1**).

Together, several studies have used MALDI-MS imaging to investigate senile plaques in tg mice and AD brain tissue. The studies have been performed over many years and a notable difference can be observed across the studies (**Table 1-1**). Part of these have been general methodological improvements in the MALDI-MS imaging field such as optimization of the sample preparation and instrumentational equipment. The studies have focused on elucidating unknown features that are associated with senile plaques such as detection of co-localizing Aβ species or using high spatial resolution imaging

to detect differences in the lipid composition across senile plaques. LMD has been used as a tool to enrich plaque regions and to increase the validity of the detected peptides (both Aβ species and lipids). Additionally, approaches that could enable detection of modified species like the pyro-glu modified Aβ have been addressed.

These improvements are crucial for ensuring detection of Aβ peptides that otherwise might be missed in MALDI-MS imaging analysis and potentially lead to false-negative conclusions. One study reported that the tgAPP$_{ArcSwe}$ mouse strain encompasses several truncated Aβ species associated with senile plaques (Carlred et al., 2016). Other studies reported that senile plaques include a limited number of Aβ species such as Aβ1-37, Aβ1-38, Aβ1-39, Aβ1-40 and Aβ1-42 and Aβ1-42 Ox using the same tg strain or tgAPP23 mice (Kaya et al., 2018; Michno et al., 2018; Stoeckli et al., 2002). Furthermore, studies investigating the senile plaque composition from AD patients have found a complex senile plaque composition that encompass a variety of modified and truncated Aβ species (**Table 1-1**; (Ikegawa et al., 2019; Kakuda et al., 2017)). Reviewing these studies indicated differences in the senile plaque composition which could be dependent on the choice of tg mouse strain or matrix. Additionally, a more complex plaque composition has been implied in AD compared to tg mice, but a direct comparison, using the same experimental setup, has not been performed and therefore was of interest in this thesis.

Table 1-1: Beta-amyloid (Aβ) species detected with MALDI-MS imaging. Ox = oxidation (M+16). Arc = peptide corresponding to mutation in the tgArcSwe mouse model. 2,5-DHA = 2,5-dihydroxyacetophenone. sDHB = super 2,5-dihydroxybenzoic acid. 3- or 11pE = truncated and pyroglutamate modified Aβ.

Study	***Species***	***Matrix***	***Aβ species***
(Stoeckli et al., 2002)	Mouse	SA	Aβ1-37, Aβ1-38, Aβ1-39, Aβ1-40, Aβ1-42, Aβ1-42 Ox.
(Rohner, Staab, & Stoeckli, 2005)	Mouse	SA, CHCA	Aβ1-37, Aβ1-38, Aβ1-39, Aβ1-40, Aβ1-42.
(Stoeckli et al., 2006)	Mouse	SA	Aβ1-37, Aβ1-38, Aβ1-39, Aβ1-40, Aβ1-42.
(Seeley & Caprioli, 2008)	Mouse	SA, CHCA, DHB	Aβ1-37, Aβ1-38, Aβ1-39, Aβ1-40, Aβ1-42.
(Kelley, Perry, Castellani, et al., 2016)	Human	DHB	Aβ1-16, Aβ1-24, Aβ5-40, Aβ14-40, Aβ1-42.
(Carlred et al., 2016)	Mouse	CHCA	Aβ1-42arc Ox, Aβ1-42arc, Aβ1-40arc $[M+Na]^+$, Aβ1-40arc, 3pE-42, Aβ1-39arc, Aβ5-43 Ox, Aβ3-40arc $[M+Na]^+$, Aβ1-38arc $[M+Na]^+$, Aβ1-38arc, Aβ2-39arc, Aβ1-37arc.
(Kakuda et al., 2017)	Human	SA	Aβx-40 and Aβx-42 (x = 1, 2, 3pE, 4, 5, 6, 7, 8, 9, 10, and 11pE), Aβ1-43.
(Kaya, Brinet, Michno, Zetterberg, et al., 2017)	Mouse	2,5-DHA	Aβ1-37, Aβ1-38, Aβ1-40.
(Kaya et al., 2018)	Mouse	2,5-DHA	Aβ1-37, Aβ1-38, Aβ1-40, Aβ1-42.
(Michno et al., 2019)	Mouse	2,5-DHA	Aβ1-37, Aβ1-38, Aβ1-39, Aβ1-40, Aβ1-42.
(Ikegawa et al., 2019)	Human	SA	Aβx-40 and Aβx-42 (x = 1, 2, 3pE, 4, 5, 6, 7, 8, 9, 10, and 11pE), Aβ1-43.
Bastrup et al, 2019 **(Publication I)**	Mouse and human	sDHB	*APPPS1-21:* mAβ11-42, Aβ8-40, Aβ1-38, mAβ1-40, Aβ1-40, mAβ1-42, Aβ1-42, Aβ1-42 Ox, Aβ1-43, Aβ1-43 Ox. *Human:* Aβ1-29, 11pE42, Aβ11-42, 11pE43, Aβ1-31, Aβ10-42,

Table 1-1 continued	Aβ9-42, Aβ1-32, Aβ8-42, Aβ8-42Ox, Aβ1-33, Aβ8-43, Aβ7-42, Aβ7-43, Aβ6-42, Aβ5-42, 3pE40, Aβ4-42, 3pE42, Aβ1-40, Aβ2-42, Aβ1-42, Aβ1-42 Ox, Aβ1-43, Aβ1-43 Ox.

1.5.2. MICROPROTEOMIC ANALYSIS OF SENILE PLAQUES

Introduction to LC-MS/MS and microproteomics

Advancements in proteomic studies in relation to liquid chromatography tandem-mass spectrometry (LC-MS/MS) have enabled high-throughput analysis platforms that are capable of elucidating complex biological systems (Pirmoradian et al., 2013). In brief, a diluted sample is eluted through an electrospray ionization (ESI) source that generates an electrospray process by subjecting a high voltage to produce polarized droplets (Wong, Meng, & Fenn, 1988; Yamashita & Fenn, 1984). The solvent flowrate ranges from low nanoliter to microliter per minute depending on factors such as used emitter, column diameter and chromatography setup. As the solvent droplets are released from the source emitter they reduce in size due to solvent evaporation. Repeatedly, the charged droplets will implode into smaller droplets because of coulombic repulsive forces and eventually become charged solvent-free ions that can be guided through the mass spectrometer (reviewed by (Ho et al., 2003; Wilm, 2011)). ESI is characterized as a soft ionization technique with generation of multiple charged ion species which is different from MALDI-MS that generally produce single charged molecular ions. For proteomic applications several mass analyzer configurations can be applied. Most state-of-the-art mass spectrometers are equipped with a mass analyzer that is TOF- or orbitrap-based (Meier et al., 2018; Scheltema et al., 2014). The orbitrap uses an electric field to trap ions in an orbital motion. In the latter, the frequency of rotation is related to the m/z ratio and thus used to determine the m/z value of the ions (reviewed by (Xuemei Han, Aslanian, & Yates, 2008)).

Two proteomic approaches are generally used; top-down and bottom-up. In top-down proteomics, an intact protein is separated by LC, electrosprayed and analyzed by a

mass spectrometer (reviewed by (Aebersold & Mann, 2016)). In contrast, the bottom-up workflow begins with digestion of a protein mixture using a sequence specific enzyme such as trypsin, followed by LC separation, electrospray ionization and analysis by the mass spectrometer (**Figure 1-6**). The bottom-up acquisition is typically achieved with one of three common strategies; data-dependent acquisition (DDA), targeted, and data-independent acquisition (DIA; (Aebersold & Mann, 2016)). As the DDA method and the closely related parallel accumulation serial fragmentation (PASEF; (Meier et al., 2018)) method were used in this PhD thesis, the focus will be on these workflows in the following section.

In brief, the DDA method on a mass spectrometer can be divided into two processes: first, a collection of ionized peptides within a full spectrum (also referred to as MS1 level) is used for selection of precursor ions. Second, a collection of precursor ions is subjected to fragmentation, typically by collision-induced dissociation (CID) or higher-energy collisional dissociation (HCD) to create a fragmentation spectrum (also referred to as MS2 level) (reviewed by (Aebersold & Mann, 2016)). The data can be analyzed by protein identification algorithms that use peptide and protein databases to identify the fragmented peptides. Other software's can be used to statistically evaluate the identified proteins. As thousands of MS1 and MS2 events can be acquired from a single specimen, the DDA method has the capability of detecting thousands of proteins in one single analysis. Therefore, the DDA approach enables system-wide identification of biological systems by detecting changes in relative protein levels and direct protein-protein interactions (Choudhary & Mann, 2010). Subsequent analysis software with the STRING database as an example can be applied to map protein interactions by using direct and indirect associations (Szklarczyk et al., 2015). Furthermore, advanced developments have enabled interpretation of PTM fragmentation spectra, enabling both protein and PTM identification within a single dataset (Xi Han, He, Xin, Shan, & Ma, 2011; Nasiri Kenari et al., 2019). These technologies allow for large-scale proteomic studies that can elucidate complex molecular networks that previously were not feasible.

To elucidate protein networks, it can be an advantageous approach to accumulate and enrich a sample specimen of interest, prior to the mass spectrometry analysis. This increases the chance of detecting the central components in a network while limiting the inclusion of "irrelevant" proteins that can make the data interpretation difficult. As an example, complex pathologies like carcinomas can be critically enhanced by including normal surrounding tissue (De Marchi et al., 2016). LMD can greatly reduce such complexity by isolating homogenous sets of biological material interest from tissue sections and can be used to accumulate specific histological environments such as senile plaques that subsequently can be prepared for MS analysis (Lutz & Peng, 2018). The amount of microdissected material in each sample can be minimal (e.g. nanogram-microgram range), hence the name microproteomics.

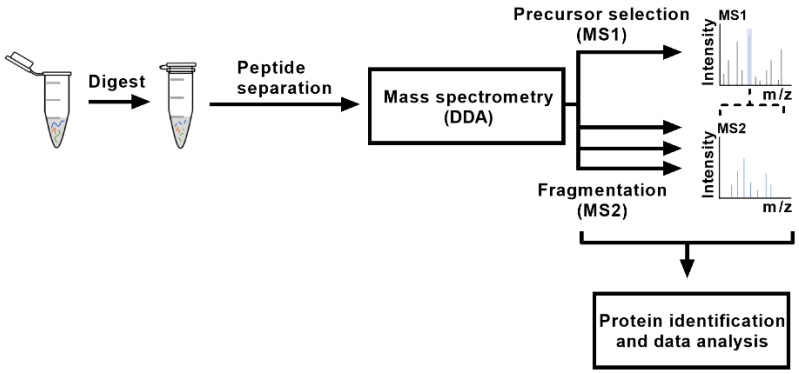

Figure 1-6: Representation of a bottom-up workflow using the data-dependent acquisition (DDA) method. A protein mixture is digested by addition of a protease and peptides are separated using liquid chromatography (LC) followed by ionization and mass spectrometry analysis. Here, precursor ions are selected (MS1) and fragmented (MS2). The generated data is analyzed to identify features such as protein IDs, relative quantification intensities and pathway associations. The figure was made by Joakim Bastrup.

Microproteomic analysis of senile plaques

Several proteomic studies have compared brain (or regional) homogenates from post-mortem AD patients to control and identified differences in signaling pathways (Johnson et al., 2018; Seyfried et al., 2017). However, it is reasoned that proteomic changes related to senile plaques are difficult to extract from such data because of its relative limited presence compared to the remaining surrounding tissue that includes a heterogenous cell population. Plaque-associated changes may therefore be lost when analyzing whole tissue homogenates, supporting the use of microdissection. In 2004, such an approach was used by Liao and colleagues who dissected and studied thioflavin-S stained senile plaque and non-plaque material from two AD patients (10 µm tissue section thickness (Liao et al., 2004)). Using LC-MS/MS analysis, 256 proteins were found to be shared between the plaque extracts from the two patients. Of these, 26 proteins were found to be enriched in senile plaques compared to non-plaque control regions. On the technical side, samples were separated on an SDS-gel and in-gel trypsin digestion was used. Approximately 500 senile plaques were extracted per sample and analysis was performed on an LCQ-DECA XP-Plus ion mass spectrometer (Liao et al., 2004). Additionally, the Sequest algorithm software (Eng, McCormack, & Yates, 1994) was used for the proteome analysis (**Table 1-2**).

In 2017, Drummond and colleagues used microdissection to extract antibody stained senile plaques from rapidly progressive (n = 22) and SAD patients (n = 22) (8 µm tissue section thickness) (Drummond et al., 2017). In total, 279 proteins were consistently identified from every patient using LC-MS/MS analysis. FFPE tissue was used with pretreatment (deparaffinization and formic acid) and between 733 and 751 senile plaques, were extracted per sample. Mass spectrometry analysis was achieved on a Q Exactive mass spectrometer instrument and the label-free quantification (LFQ) analysis was performed with MaxQuant and subsequently Perseus for bioinformatic analysis (Drummond et al., 2017).

Table 1-2. Comparison of microproteomic studies analyzing the senile plaque proteome. SAD = sporadic Alzheimer's disease. APPPS1-21 = transgenic mouse model of AD bearing mutations in the APP and PSEN1 genes.

Study	***Tissue type***	***Tissue section thickness***	***Plaque extract number per sample***	***Average plaque diameter***	***Consistent plaque proteins***
(Liao et al., 2004)	AD (n = 2)	10 µm	500	NA	188
(Drummond et al., 2017)	SAD (n = 22)	8 µm	733 - 751	~61 µm	279
(Xiong, Ge, & Ma, 2019)	AD (n = 3) & APPPS1-21 (n = 6)	35 µm	3000	80 - 100 µm	AD = 3848 & APPPS1-21 = NA
Bastrup et al, 2019 (Publication II)	APPPS1-21 (n = 6)	25 µm	300	~85 µm	183

In 2019, Xiong and colleagues used microdissection to extract stained senile plaques (Amylo-Glo RTD plaque staining reagent, Biosensis) from three AD patients, three age-matched healthy controls, six tgAPPPS1 mice and three non-tg wildtype littermates (~12.5-month-old mice; 35 µm tissue section thickness) (Xiong et al., 2019). The study identified close to 4000 proteins that were consistent across senile plaque samples from the three AD patients. By comparing senile plaque extracts to adjacent control regions in both tgAPPPS1-21 mice and AD, they identified distinct patterns of regulated pathways (Xiong et al., 2019). In tgAPPPS1-21 mice, proteins associated with TYROBP causal network, microglia pathogen phagocytosis pathway, complement and coagulation cascade were mostly regulated. Proteins associated with complement activation, inflammatory response and allograft rejection were mostly regulated in AD samples (Xiong et al., 2019). Based on these findings, the study concluded that the protein composition in senile plaques from tgAPPPS1-21 mice and AD patients was different. Notably, the diameter of each extracts was 80-100 µm with approximately 3000 dissections from each brain sample resulting in a large amount of starting material (≥ previous studies, including our work in publication II). Tandem

mass tag (TMT)-labeling was used, samples were analyzed on an Orbitrap Fusion Lumos Tribrid Mass spectrometer and quantification analysis was performed with the Proteome Discoverer software (Xiong et al., 2019).

Together, these studies have observed that senile plaque extracts encompass 100-1000s of proteins in both the tgAPPPS1-21 mouse and AD brains, despite the use of different mass spectrometry instruments and identification software (**Table 1-2**). Approximately 256 - 279 plaque-associated proteins have consistently been observed in studies when extracting between 500 and 751 extracts from AD patients, respectively (Drummond et al., 2017; Liao et al., 2004). A recent study identified 3848 proteins when increasing both the tissue thickness to 35 µm and the number of extracted plaques to approximately 3000 (**Table 1-2**; (Xiong et al., 2019)).

The microproteomic approach in the three studies listed here have been used to describe the current molecular processes occurring within and around senile plaques by associating the proteins to pathways and cellular compartments. Furthermore, the co-localization of several proteins has been validated by fluorescent immunohistochemistry and microscopy imaging (Drummond et al., 2017; Liao et al., 2004). The imaging analysis has been based on objective lenses with a 20X-40X magnification and the validation has therefore been focused on co-localization rather than co-aggregation with Aβ because of the limited degree of high resolution by these objective lenses.

PTM analysis of the dissected senile plaque material has not been investigated in these studies (Drummond et al., 2017; Liao et al., 2004; Xiong et al., 2019). Since aggregated Aβ peptides have been reported to encompass a variety of different PTMs, it is considered relevant to apply the algorithms that enables PTM identification of the proteomic data due to their possible pathological involvement (See sections, **Amyloid-β peptides, aggregation and senile plaque deposition**, and **Introduction to LC-MS/MS and microproteomics**).

[Page left blank intentionally]

CHAPTER 2. OBJECTIVES

AD is currently one of the biggest healthcare challenges worldwide, but despite several clinical trials no disease modifying treatments are available for treating the devastating disease. Senile plaques are one of the major hallmarks of AD and thought to be critically involved in the initial stages of AD pathogenesis. Understanding the molecular complexity of senile plaques may enable identification of targets that can lead to novel treatment strategies. MALDI-MS imaging is an emerging technology that enables label-free detection, identification and distribution of molecules. Previous studies using MALDI-MS imaging, have reported a diverse senile plaque composition which highlights the importance of optimizing the method to increase sensitivity and detection of Aβ species.

New improvements in microproteomics enable unbiased identification of biological systems and can be used to understand the local proteomic processes occurring within and around senile plaques. Recent advancements in PTM analysis enables PTM analysis within LFQ data and thus creates a possibility of adding another dimension to the protein analysis. It is thought that such additional information could be valuable for treatment strategies targeting Aβ and senile plaques.

This PhD thesis aimed to use MALDI-MS imaging and a microproteomic approach to investigate the underlying molecular features of senile plaques in AD and tgAPPPS1-21 mice. These technologies have been used to study the peptidomic and proteomic alterations in AD and tgAPPPS1-21 brain tissue. Additionally, microscopy imaging analysis has been used to validate the plaque-association of two proteins that were identified by our microproteomic approach. Two chronic antibody treatment studies with gantenerumab and aducanumab targeting different Aβ epitopes have been performed in tgAPPPS1-21 mice to elucidate the modulation of clearance mechanisms and of the protein composition of senile plaques.

Overall objectives:

I. Determine the peptidomic profile of Aβ species in senile plaques from AD and tgAPPPS1-21 mouse brains (included in publication I).

II. Determine the proteomic profile, including PTMs, of senile plaques compared to surrounding tissue in tgAPPPS1-21 mouse brains (included in publication II). Investigate the senile plaque-association of selected identified proteins by microscopy imaging (included as preliminary data).

III. Determine the proteomic profile of senile plaques after an anti-Aβ antibody treatment targeting Aβ in the tgAPPPS1-21 mice (included in manuscript III).

CHAPTER 3. METHODOLOGICAL CONSIDERATIONS

This chapter describes the methodological considerations that were utilized in the course of this PhD work. These explanations are referring to the experiments in the publications and manuscript. A description of the experimental methods and materials is provided in the attached publications and manuscript.

3.1. CHOICE OF MOUSE MODEL

The generation of several tg amyloid-models is based on FAD mutations like the mutations in the *APP*, *PSEN1*, or *PSEN2* genes. For this PhD thesis the tgAPPPS1-21 strain was used because of its robust Aβ accumulation and well-characterized phenotype that has been widely used in previous studies, including treatment studies (Bittner et al., 2012; Radde et al., 2006; Ulrich et al., 2014). The tgAPPPS1-21 strain is created on a C57BL/6J genetic background and designed with the Swedish mutation in the *APP* gene (K670/671NL) as well as a mutation in the *PSEN1* gene (L166P). These mutations cause increased production and accumulation of Aβ peptides that can be detected in the neocortex after approximately six weeks of age (Radde et al., 2006). The brain levels of Aβ1-42 is higher compared to Aβ1-40 which is similar to the Aβ1-42/Aβ1-40 ratio observed in CSF from AD patients (Radde et al., 2006). Early signs of neurodegeneration measured on dendritic spine loss can be observed after approximately 10 weeks. For the studies described in this thesis, female mice were used in the age range from 8- to 12 months. This age range was chosen for two main reasons: 1) the mice have excessive senile plaque deposition in the entire brain enabling the possibility of analyzing specific brain regions such as the cerebral cortex or hippocampus, and 2) ensuring a possibility of comparison to longitudinal antibody-treatment studies. It was decided to focus on female mice to avoid a potential gender-associated difference and because female tgAPPPS1-21 mice have been reported to

express a higher senile plaques load compared to male tgAPPPS1-21 mice (Ulrich et al., 2014).

3.2. SENILE PLAQUE STAINING METHODS

Senile plaques are usually distinguishable by their morphology in which they are referred to as "primitive", "classic" or "compact/burned out" (Probst et al., 1987). Based on these morphological differences, several staining methods were considered prior to the experiments. For example, staining with fluorescent dyes can detect protein aggregates by interacting with beta sheet structures such as congo red and thioflavin-S or -T. Additionally, Aβ targeting antibodies like 6E10 (BioLegend) or D54D2 (Ambient), can bind to specific Aβ epitopes and therefore both methods have advantages and disadvantages. Stainings using the fluorescent dyes for aggregated proteins are relatively fast (~30 minutes) and easy to apply but increase the risk of false-positive inclusion of other proteins due to unspecific binding of β-sheet conformational structures. On the other hand, immunostainings with anti-Aβ antibodies are specific but more labor intensive with several longer incubation times and buffer changes (days). Therefore, thioflavin -T and -S stainings were preferred prior to mass spectrometry analysis (when using the LMD approach). Notably, diffuse plaques are weakly stained by thioflavin and therefore most detected plaques are neuritic when using this dye (Bussière et al., 2004). To limit the risk of including false-positive regions, careful examination of plaque-morphology was also applied by using a 20X objective lens. Furthermore, a head-to-head comparison of the thioflavin-T and 6E10 staining was performed on adjacent tgAPPPS1-21 mouse brain tissue sections in publication II, validating that senile plaques were exclusively visualized by thioflavin-T.

3.3. MALDI-MS IMAGING EXPERIMENTS

Several MALDI-MS imaging studies have visualized senile plaques and reported a diverse plaque composition (See section, **MALDI-MS imaging of senile plaques**). Notably, different matrices have been used while the matrix additives have been limited to TFA. PA has been reported to reduce signal suppression effects in MALDI-

MS studies and it was therefore hypothesized that adding this matrix additive to the sDHB matrix could increase the S/N ratio of Aβ peptides. It was decided to use a low spatial resolution for the comparison to the other matrices (CHCA/TFA, SA/TFA, sDHB/TFA) to limit matrix deterioration and thus a potential bias.

The sublimation deposition approach has been used to study senile plaques (Kelley, Perry, Castellani, et al., 2016). Sublimation results in a uniform and homogenous crystal layer with limited risk of analyte diffusion. The reproducibility between sublimation and automatic sprayers such as the ImagePrep, have been found to be similar (Gemperline, Rawson, & Li, 2014). However, the ImagePrep sprayer enables the possibility of controlling the matrix thickness and wetness by an optical sensor that monitors light scattering from the matrix during the deposition. Both factors affect the efficiency of analyte extraction and incorporation into the matrix microcrystal lattice. As the aim in publication I was to compare matrices across several brain sections, this feature was found important to ensure a reliable comparison.

The Ultraflextreme instrument has been widely used in previous studies investigating senile plaques in tg mouse models and AD brain tissue. We similarly used this instrument in our analysis and used the software, SCiLS Lab (Bruker Daltonics), to process and analyze the MALDI-MS imaging data. SCiLS Lab includes tools like mass spectral pre-processing, spatial visualization, principal component analysis (PCA), clustering analysis, statistical analysis, identification of discriminative m/z values between samples and detailed peak reports that were found useful in the analysis. For example, the top hat baseline pre-processing feature was used in this work because of the ability to reduce and smooth the baseline. Additionally, the total ion count (or current) (TIC) normalization method was used for spectral comparison.

3.4. MICROPROTEOMIC STRATEGY

Microdissection and LC-MS/MS analysis of senile plaques has been achieved in both fresh frozen and FFPE tissue (Drummond et al., 2017; Xiong et al., 2019). A study observed that LC-MS/MS analysis of FFPE preserved tissue increased the number of artificial modifications compared to fresh frozen tissue (Bennike et al., 2016). Based on this observation and our aim to detect modifications on proteins co-localizing with

senile plaques, it was decided to use fresh frozen tissue. Our study differed from the previously mentioned plaque-analyzing studies in that: 1) We used a detergent enhanced solubilization strategy with low volume acid-labile surfactant. 2) We used 25-um-thick tissue sections for microdissection. 3) We used a match-between-run strategy matching ID's to a pooled higher intensity sample. The previous plaque-analyzing studies have used tissue sections of different thickness: 8-, 10- and 35-µm (**Table 1-2**; (Drummond et al., 2017; Liao et al., 2004; Xiong et al., 2019)). Senile plaques vary in size (10 – 100 µm in diameter) and so care was taken to ensure the quality of the microdissection. For example, when increasing the tissue thickness and microdissection area, the risk of including surrounding non-plaque tissue also increases. Based on this reasoning, it was decided to use 25-µm-thick tissue section and keep the dissection area close the senile plaque periphery.

Senile plaque reduction was observed in the hippocampal region of the aducanumab treated mice which limited the area that could be used for microdissection in the samples. The increased sensitivity of the trapped ion mobility spectrometry (Tims)-TOF Pro instrument compared to Q-Exactive HF-X was therefore considered to be advantageous because of the limited sample amount that was acquired in the microdissection from the aducanumab study (~90 and 300 plaque dissections per sample in manuscript III and publication II, respectively). Additionally, a direct infusion setup was used in manuscript III to increase the sensitivity even further.

3.5. ANTIBODY TREATMENT STUDY DESIGN

Two chronic anti-Aβ antibody treatment studies using gantenerumab and aducanumab were performed during the PhD work. The antibody treatment strategies were based on previous publications as well as in-house experience. Bohrmann and colleagues used tgPS2APP mice that were 5- to 6-months old and administered a weekly dose of gantenerumab for 5-months (20 mg/kg body weight; human IgG1 backbone; intravenous (i.v.) via the tail vein) (Bohrmann & Baumann, 2012). Similarly, Jacobsen and colleagues performed a chronic study with weekly dosing of gantenerumab (20 mg/kg body weight) in tgAPP_{London} mice (human APP isoform 695 with London mutation V717I). The mice were 13.5-month-old at beginning of dosing

and treated for 4-months (Jacobsen et al., 2014). Based on these studies, it was decided to use 4-month old tgAPPPS1-21 mice and to apply the same chronic dosing strategy of gantenerumab in this PhD work (weekly administration, 20 mg/kg, i.v.; 4-month administration, mouse IgG2a backbone). Notably, the senile plaque deposition can be observed after approximately 9- and 10-months of age in the tgPS2APP and $tgAPP_{London}$ model, respectively. Therefore, 4-months of age was chosen because the tgAPPPS1-21 mice start to show a robust plaque deposition at this age. In tgAPPPS1-21 mice, senile plaque deposition can already be observed after approximately 1.5-months of age in the cortex while the deposition in hippocampus begins after 3- to 4-months (Radde et al., 2006).

In 2016, Sevigny and colleagues reported that a weekly dose of chimeric (ch) aducanumab for 6-months significantly reduced the senile plaque load in 9.5-month old tg2576 mice (Sevigny et al., 2016). The antibody was administered by intraperitoneal (i.p.) delivery and was most efficacious at the 10 and 30 mg/kg per doses (Sevigny et al., 2016). A chronic study in-house using a weekly dose (10 mg/kg; i.p.) in 6-month old tgAPPPS1-21 mice observed significant reduction of senile plaques in both cortex and hippocampus after a 4-month treatment (personal communication with Dr. Lone Helboe, H. Lundbeck A/S). Based on the successful in-house data, it was decided to replicate that study design (weekly dose of aducanumab; 10 mg/kg; human IgG1 backbone; i.p.; tgAPPPS1-21 mice; 6-month of age at the beginning of the study; 4-month duration).

Two control groups were used in both antibody treatment studies in this PhD work; one treated with PBS and one treated with a non-targeting and isotype control (IgG1). Mice were group housed, provided with enrichment, and had access to water and food ad-libitum. The administration methods were practiced on another cohort of mice prior to the two antibody studies to limit any effects of animal handling such as stress and other confounding factors that could affect the study outcome.

3.6. AN IMAGING APPROACH TO VALIDATE IDENTIFIED SENILE PLAQUE PROTEINS

We decided to use a novel technique called protein-retention expansion microscopy (ProExM) to validate the presence of two proteins that were identified in the microproteomic approach (publication II). ProExM involves incorporation of a swellable gel that can be utilized to physically enlarge a specimen (Chen, Tillberg, & Boyden, 2015). The technique results in a 4-5 times isotropic expansion that enables imaging at nanoscale resolution with conventional microscopical equipment. Recent methodological advancements have included anchoring of conventional antibodies into the swellable gel and thereby allowed the use of regular fluorescent antibody staining (Tillberg et al., 2016) (**Figure 3-1**).

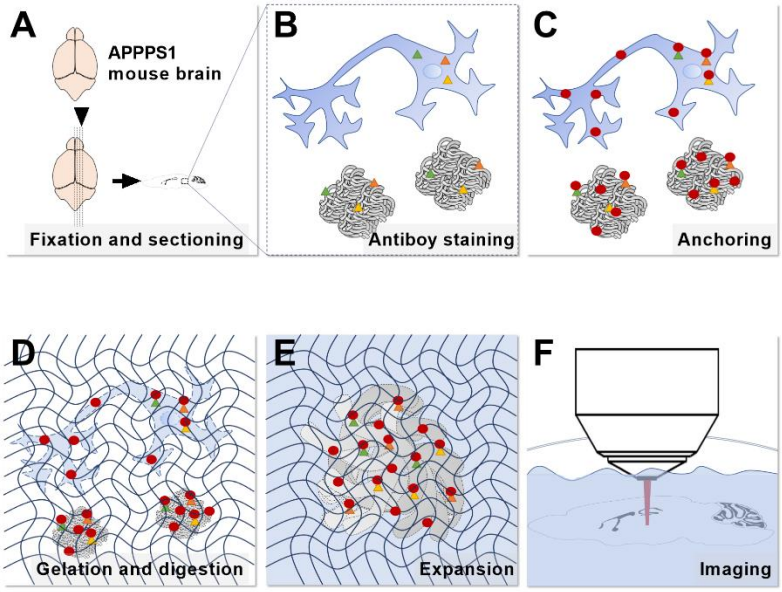

Figure 3-1: Methodological workflow of protein-retention expansion microscopy (ProExM). Mouse brain is fixed in paraformaldehyde (PFA) and sectioned into 100 µm tissue thickness. B) Antigen retrieval with formic acid and heat to increase penetration of antibodies used for immunostaining (triangles). C) Amines on biomolecules are modified with acryloyl-X (circle) to create an acrylamide group that

subsequently is incorporated into the gel (Tillberg et al., 2016). D) Triggering of gelation and subsequent digestion using Proteinase K. E) Expansion of tissue section when incubating in water. F) imaging with confocal setup using a water-immersion objective lens (20X/1.0). The figure was made by Joakim Bastrup.

Senile plaques can vary greatly in size (10-100 µm in diameter) and inclusion of thick tissue sections are therefore advantageous when imaging senile plaques in their unity. On the other hand, immunohistochemistry of thick tissue sections can introduce several staining issues by poor antibody penetration. It was therefore decided to use 100 µm thick tissue sections and two antigen retrieval steps prior to immunostaining; 1) incubation in formic acid (80%) and 2) treatment with a detergent-rich buffer and heat. Additionally, we used four days of incubation with primary antibodies. We found that these steps combined, resulted in an efficient staining when using primary antibodies like the 6E10 (anti beta-amyloid), GA524 (astrocyte marker) and Ab5076 (microglia marker; data not shown). Although several different microscopic approaches such as light-sheet or super-resolution techniques could have been used to image the stained and expanded tissue-gels, we found that an upright confocal microscope was most beneficial (for example due to the capability of fast orientation within the expanded tissue). The system was equipped with a water-immersion 20X/1.0 objective lens with high working distance (WD; 2 mm). The relative low resolution but high numerical aperture (NA) and WD was found to be advantageous because the expansion factor provided morphological details that could be detected by the high NA while the WD enabled acquisition throughout the expanded samples. The image analysis was performed in ZEN (Zeiss), ImageJ and Imaris (Bitplane).

[Page left blank intentionally]

CHAPTER 4. RESULTS AND DISCUSSION

4.1. MAIN FINDINGS

This chapter focuses on the main findings and novelty from the publications and manuscript written during the PhD project. Additionally, preliminary data from the ProExM experiments are included. The chapter ends with a general discussion of the main findings and how these findings from tgAPPPS1-21 mice can be related with AD pathology.

4.1.1. PUBLICATION I

In publication I we reported a dual strategy that used two approaches to reduce signal suppression effects and increase detection of Aβ peptides in MALDI-MS imaging. We found that a parallel approach with LMD and PA together with the sDHB matrix greatly improved the S/N of Aβ peptides from senile plaques from both AD and tgAPPPS1-21 mouse brain tissue sections. The positive effect on ionization by PA as matrix additive to the sDHB matrix was particularly relevant when studying AD brain tissue. We observed a highly complex Aβ plaque composition with high levels of truncated and modified forms such as pyro-glu modified Aβ which was not observed in the tgAPPPS1-21 mice. The data indicated that tgAPPPS1-21 mice express a less complex senile plaque Aβ peptide profile compared to AD.

4.1.2. PUBLICATION II

In publication II we reported a microproteomic strategy to identify and analyze proteins co-localizing with Aβ in senile plaques isolated from the tgAPPPS1-21 mice. Three regions: senile plaques, adjacent control regions from tgAPPPS1-21 mice and similar regions from wildtype littermates, were microdissected and analyzed. This approach enabled characterization of molecular processes occurring within and around senile plaques, including identification of unique PTM profiles. Our approach

identified 183 proteins that were consistently observed across senile plaque extracts. By using LFQ, we identified 27 proteins co-localizing with senile plaques that were significantly regulated when comparing senile plaques to adjacent control regions. These proteins indicated different biological processes in which the upregulated proteins were associated with endocytosis and metabolism, and the downregulated proteins were associated with neuronal cytoskeleton. Our unbiased PTM analysis identified 193 and 117 modifications that were exclusive to proteins co-localizing with either senile plaques or adjacent control extracts, respectively. The identification of such exclusive PTMs is a novel finding and adds an additional layer of complexity to senile plaques from tgAPPPS1-21 mice that we are the first to address.

4.1.3. VALIDATION OF TWO IDENTIFIED PLAQUE-ASSOCIATED PROTEINS

Our microproteomic data supports the notion that a complex interplay between plaque and brain cells was occurring. We reasoned that detailed imaging techniques could elucidate this interaction better. For example, super-resolution techniques have successfully visualized nanoscale details of amyloid fibrils in both tgAPP mice and AD brain using antibody staining (Blazquez-Llorca, Merchán-Pérez, Rodríguez, Gascón, & DeFelipe, 2013; Mlodzianoski et al., 2019; Querol-Vilaseca et al., 2019). However, super-resolution techniques are challenged by penetration depth in tissue (very high magnification objective lenses depend on the use of short WD). This limitation becomes specifically relevant when imaging matured plaque structures that can reach up to 100 µm in diameter. Based on these challenges, we turned to ExM (Chen et al., 2015). This method has been reported to enable physical expansion of tissue sections by approximately 4-5 times the original size. The method is based on linking water-absorbing polymers to biomolecules within a tissue section, which enables expansion once exposed to water. Since most of the tissue will contain water, the tissue specimen becomes transparent which is favorable for imaging thick tissue sections (Chen et al., 2015). A recent optimization of the method, enabled incorporation of antibodies to the polymers, enabling combination with fluorescent immunohistochemistry (Tillberg et al., 2016) (**Figure 3-1** in previous chapter).

The remaining section focuses on preliminary data that were acquired with this technique. We are the first to report that the ProExM protocol can be applied on senile plaques from tgAPPPS1-21 mice.

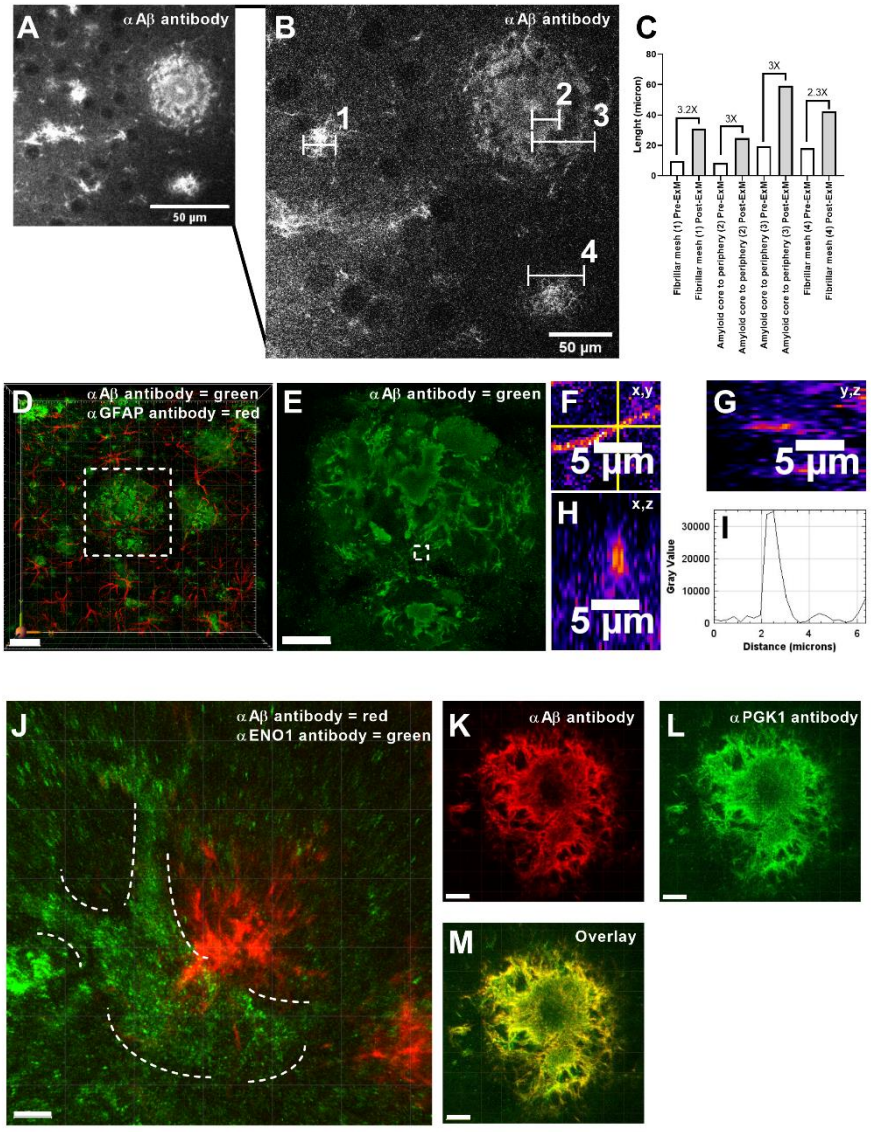

Figure 4-1: Validation of protein-retention expansion microscopy (ProExM) method on senile plaques in transgenic APPPS1-21 mouse brain sections. Anti-beta-amyloid (Aβ) immunostaining before A) and after B) ProExM protocol. C) Representation of

distance measurements and calculated expansion factor in A) and B). White lines indicate amyloid structures that were measured. Images were acquired with the same water-immersion objective lens (20X/1.0) and settings. Scale bar 50 µm. D) Tilescan stack (3x3) of expanded tissue (beta-amyloid (Aβ; green; 6E10, BioLegend) and astrocytes (red; GA524, DAKO)). Scale bar = 100 µm. E) Single-plane images of region of interest (white box in D). Scalebar = 50 µm. F-H) shows orthogonal view of Aβ fibril in E) (within white box). Scalebar = 5 µm. I) Plot profile illustrating the diameter (x,y dimension) of the selected Aβ fibril in F). J) Double immunostaining of Aβ (red) and enolase-1 (ENO1, Santa-Cruz) protein (green). Cellular morphology is indicated by dotted lines. Scale bar 10 µm. K-L) Double immunostaining of Aβ K) and phosphoglycerate kinase 1 (PGK1, Santa-Cruz; L). M) Overlay of K) and L). Scale bar = 20 µm.

We found that including antigen retrieval prior to immunostaining, increased the penetration depth of antibodies (data not shown). Furthermore, we compared a section stained with an anti-Aβ antibody (6E10, BioLegend) before and after expansion. This enabled us to compare and measure the expansion factor, which in this case was found to be approximately three times the original size (**Figure 4-1A-C**). After establishing that ProExM could expand senile plaques, we investigated the capability of resolving fine amyloid structures. By using a tile-scan function, we were able to resolve both mature plaques and association to surrounding astrocytes (GA524 antibody, DAKO) as well as fine structures such as Aβ fibrils (**Figure 4-1D,E**). The diameter of these fibrils was approximately 1 mm (x,y dimension), meaning that the ProExM method could resolve structures between 200-300 nm when extracting the expansion factor (**Figure 4-1E-I**).

Using this method, we investigated whether we could detect two proteins co-localizing in senile plaques that were identified in publication II. Enolase-1 (ENO1) and phosphoglycerate kinase 1 (PGK1) are both associated with glycolysis (Kim & Dang, 2005). We observed that ENO1 (sc-271384, Santa-Cruz) immunoreactivity was localized next to senile plaques (**Figure 4-1J**), suggesting it may be expressed in the surrounding glia. On the other hand, PGK1 (sc-48342, Santa-Cruz) was highly co-

localized with senile plaques (**Figure 4-1K-M**) suggesting a true-plaque association. These findings underlined the importance of validating the precise localization of proteins by imaging techniques following their identification by MS. A description of the protocol is included in (**Appendix A**).

4.1.4. MANUSCRIPT III

In manuscript III we reported an MS-based investigation of proteomic patterns associated with senile plaque extracts and surrounding tissue in tgAPPPS1-21 mice after treatment with an anti-Aβ targeting antibody. Initially, we determined the treatment effect of two antibodies, gantenerumab and aducanumab, by measuring the senile plaque load with thioflavin-S. We identified a significant reduction of senile plaques in the hippocampal brain region of tgAPPPS1-21 mice treated with aducanumab compared to controls and focused on this area in the subsequent microproteomic analysis. Additionally, we utilized MALDI-MS imaging to investigate the senile plaque composition in the frontal cortex of the tgAPPPS1-21 mice that supported a limited effect of the antibody in the cortical regions. Our microproteomic strategy of the hippocampus was based on three tissue extracts: senile plaque, senile plaque penumbra, and an additional ring to the penumbra (referred to as SP, SPP-L1, and SPP-L2 in manuscript III). We identified a proteomic similarity between the respective subregions, as several proteins were shared. For example, 216, 315 and 395 proteins were detected in SP, SPP-L1, and SPP-L2 extracts from the three treatment groups, respectively. However, our statistical analysis identified that these proteins (especially in SPP-L1 and SPP-L2 subregions) were regulated when comparing the respective LFQ levels across the groups. Here, a difference was observed in the SPP-L1 and SPP-L2 subregions between the treatment groups where we identified 18 and 15 differentiating proteins, respectively. Using pathway analysis, we associated these proteins to different pathways and found that proteins related to energy metabolism were increased in tgAPPPS1-21 mice dosed with aducanumab. Furthermore, an increased regulation of the astrocytic marker, glial fibrillary acidic protein (GFAP), was observed in SPP-L1 regions from aducanumab treated mice compared to the unspecific IgG group. Our data suggested increased recruitment of

glia cells to senile plaques in the aducanumab treated mice. Interestingly, we also observed differences in proteomic patterns of nucleoside diphosphate kinase A (NME1) and syntenin-1 (SDCBP) across the subregions within each treatment group. These are GTPase regulating proteins and have been reported to be involved in phagocytosis, endocytosis and lysosomal degradation. The regulation of these proteins was mainly observed in aducanumab treated mice and could explain part of the plaque degradation caused by aducanumab's action.

4.2. DISCUSSION OF MAIN FINDINGS AND ASSOCIATION WITH AD

The work presented focused on elucidating the underlying molecular complexity of senile plaques in AD and tgAPPPS1-21 mice. We investigated this at a peptidomic level in publication I where we observed a variety of Aβ peptides co-localizing with Aβ1-42 in both AD and tgAPPPS1-21 mouse brains using an optimized MADLI-MS imaging protocol. Our parallel approach with PA and LMD increased the detection of Aβ proteoforms, including pyro-glu modified species in brain tissue from AD patients. The detection of pyro-glu modified Aβ in AD brain tissue was recently reported with SA as matrix and vapor pretreatment with formic acid (Kakuda et al., 2017). Notably, we detected this modification when using PA as additive to the sDHB matrix without pretreatment, indicating an advantage of using PA. Matrix additive variants were previously reported to improve ion formation and S/N ratio of phosphopeptides and non-phosphopeptides in a direct comparison to PA (Kuyama et al., 2008). Thus, we consider that using e.g. methanediphophonic acid in combination with the sDHB matrix might improve the S/N ratio of Aβ proteoforms even further.

Senile plaques in tgAPPPS1-21 mice encompassed mainly full-length peptides such as Aβ1-40, Aβ1-42 and Aβ1-43 while senile plaques in AD brain tissue encompassed a variety of truncated and modified Aβ species. Thus, a central difference in the senile plaque composition was observed in the brains of tgAPPPS1-21 mice and AD patients. We reason that this observation could be due to several factors such as: 1) Aβ peptides are reported to be processed by extracellular proteases, possibly leading to truncated forms (Cataldo, Thayer, Bird, Wheelock, & Nixon, 1990; Smith, Kalaria,

& Perry, 1993). However, the aggressive overproduction of Aβ in combination with rapid fibril formation (the kinetics of Aβ) might hamper such processing by rapid aggregation which could result in a rapid senile plaque deposition in the tgAPPPS1-21 mice and explain the relative high levels of full-length Aβ peptides. 2) Multiple enzymes are involved in cleavage of Aβ in AD. It might be that part of these are missing or reduced in the tgAPPPS1-21 mice which similarly could lead to deposition of full-length Aβ peptides. Despite these differences the tgAPPPS-21 model did express an abundant level of Aβ1-42 within senile plaques which was also observed as the most abundant species in AD brains and supports its applicability.

Recent in-house immunohistochemistry data showed minimal reactivity of antibodies targeting pyro-glu modified Aβ in 9-month old tgAPPPS1-21 mice while a higher reactivity was observed in 12-month old mice (data not shown, personal communication Dr. Lone Helboe, H. Lundbeck A/S). This finding was in line with our observation of lacking pyro-glu modified Aβ in 9-month old tgAPPPS1-21 mice. We have not analyzed 12-month old tgAPPPS1-21 mice but consider that the modification might be detectable in older mice with MALDI-MS imaging. We reason that the appearance of this modification could be considered in future studies using the tgAPPPS-21 mouse strain given the likely involvement of pyro-glu modified Aβ species in AD. Furthermore, the Aβ species profile could be investigated further as these appear to be a central difference between senile plaques from tgAPPPS1-21 and AD brains. The tgAPPPS1-21 mouse strain is designed to overexpress two FAD mutations that model an aggressive amyloidopathy. MALDI-MS imaging analysis of brain tissue from FAD patients carrying one of these mutations would be valuable to elucidate whether a comparable Aβ peptide composition with truncated and/or full-length Aβ peptides is observed. If so, Aβ compositions in senile plaques from FAD would differ from SAD brains and therefore it could be considered to use tgAPPPS1-21 mice prior to clinical trials focusing on treating FAD rather than SAD patients.

In publication II we applied a microproteomic strategy to investigate proteins and PTMs in senile plaques and surrounding tissue extracts from tgAPPPS1-21 mice. We identified 22 up- and 5 downregulated proteins by comparing proteome data from senile plaques and surrounding tissue. Using literature-based pathway analysis, we

observed that the upregulated proteins were associated with metabolic pathways (e.g. glycolysis), endocytosis and vesicle-transport, implying that several regulatory processes were occurring within the senile plaques. This approach was considered valuable due to the possibility of determining protein changes associated with plaque-brain interaction pathways which were necessary for answering objective III in the thesis. One limitation with the MS method was the lack of ability to localize the identified proteins and clarify whether they were truly associated with the senile plaques. For example, aggregated Aβ peptides are engaged by glia cells and several proteins in a microdissected plaque extract could therefore be associated with the cellular environment. This was supported by the identification of several proteins that were associated with e.g. glycolysis. Thus, it was reasoned that combination with other techniques like ProExM imaging was relevant for clarifying this association. Therefore, we optimized the ProExM protocol to enable detailed imaging of senile plaques in brain tissue from tgAPPPS1-21 mice. We clarified a distinct senile plaque-association of ENO1 and PGK1, both of which were identified in publication II and manuscript III. Our data showed that the ENO1 did not co-localize with the senile plaque structures but was associated with morphologies next to senile plaques. This observation may be explained by engaging glial cells such as microglia or astrocytes. We consider that a triple staining visualizing both Aβ, ENO1 and either microglia or astrocytes could be beneficial to confirm this finding. On the other hand, we are the first to visualize that PGK1 co-localized with amyloid aggregates. It should be emphasized that we used the same anti-mouse secondary antibodies for detecting ENO1 and PGK1 and that the gain and laser power were kept at a minimum to limit the possibility of autofluorescence or cross excitation and thus a potential false-positive detection of senile plaques. The fact that we did not detect amyloid structures with the ENO1 immunohistochemistry supports this reasoning. PGK1 is a key enzyme in glycolysis and gluconeogenesis but altered levels of this protein has previously been linked to AD pathology (Ho Kim et al., 2015). Notably, PGK1 has been reported as a cargo protein in exosomes and ectosomes (reviewed by (Meldolesi, 2018)). Glial cells release exosomes and ectosomes as part of their Aβ processing and we therefore consider that this could explain the pathway from the intracellular to the extracellular

position. Vimentin and annexin, two other cargo proteins that are also associated with exosomes and ectosomes (Meldolesi, 2018) have similarly been detected in previous LC-MS/MS studies of microdissected plaque material which supports this idea (Drummond et al., 2017; Liao et al., 2004). PGK1 was recently reported as a therapeutic target in Parkinson's disease that similarly is characterized by aggregation and deposition of α-synuclein into Lewy bodies (Cai et al., 2019). Cai and colleagues observed that treatment with terazosin increased the activity of PGK1 and enhanced glycolysis which slowed the disease progression of Parkinson's disease. Thus, we consider that treatment with terazosin may also be a therapeutic approach in AD.

Our PTM analysis identified several exclusive modifications in senile plaque extracts such as oxidation, deamidation, pyro-glu, citrullination and ISD (z + 2)-series. The ISD (z + 2)-series identification was primarily identified on proteins associated with senile plaques (12 sites vs 2 sites on proteins associated with adjacent control). These proteins were 14-3-3 protein isoforms, APP, Beta-actin-like protein 2, Excitatory amino acid transporter 2 and Tubulin alpha chain isoforms. The modification refers to one type of fragment ions observed in a tandem MS spectrum and therefore not a biological modification. This was not anticipated but we speculate that it could be due to side-chain fragmentation generating z-ions during the dissociation, although further studies are needed to elucidate this finding. Oxidation, deamidation, pyro-glu and citrullination have been associated with AD and our detection of these modifications was therefore in-line with previous findings (Adav et al., 2016; Hensley et al., 1995; Ishigami et al., 2005; Sullivan et al., 2011). Several modifications have been reported on Aβ, but the fact that proteins co-localizing with senile plaques also are subjected to modifications adds another layer of complexity that could have pathological impact. For example, an exclusive pyro-glu modification was identified on CLU in senile plaque extracts in our study. Despite the identification of *CLU* as a susceptible gene in GWAS, CLU has also been reported to co-aggregate with Aβ (Lambert et al., 2013; Oda et al., 1995). It remains to be elucidated whether such modification alters the biological function of CLU and thus also Aβ toxicity.

We identified a total of 183 proteins that were consistently observed in senile plaque extracts from the tgAPPPS1-21 mouse strain. One of the aims in publication II was to determine whether tissue-associated differences between senile plaques and adjacent control regions in the tgAPPPS1-21 also were observed in AD. At the time of our experiment three comprehensive studies that investigated the senile plaque proteome in AD patients had been published, so we compared our findings with the published data. Since approximately 70% of the detected proteins in our study were present in the consistent proteins observed by Drummond and colleagues, we considered that a general proteomic profile of senile plaques was conserved across tgAPPPS1-21 mice and AD (Drummond et al., 2017). The number of consistent proteins was lower in our study compared to recently published studies analyzing senile plaque extracts from AD brains (183 vs 188, 279 and 3848, respectively; (Drummond et al., 2017; Liao et al., 2004; Xiong et al., 2019)). This could be explained by regional and methodological differences in sample preparation, tissue thickness, mass spectrometer instrument and analyzing software as mentioned previously (See section, **Microproteomic analysis of senile plaques**).

Based on the findings from publication I and II, a central difference in the Aβ peptide profile was observed between tgAPPPS1-21 mice and AD patients while a similarity was observed at a proteomic level. Together, the data suggested that the response mechanism in the tgAPPPS1-21 mouse brain could replicate the coping mechanisms to Aβ accumulation observed in AD. This seemingly contradicting finding is critical when performing anti-Aβ treatment experiments with the tgAPPPS1-21 mouse model. On one hand, the model resembles a comparable cellular coping mechanism to Aβ accumulation. On the other hand, the model accumulates Aβ aggregates that not resemble a true-plaque peptide-composition seen in AD. Thus, it is considered that the tgAPPPS1-21 mouse is a mechanistic model of AD. It can be debated, whether the outcome of an anti-Aβ antibody treatment in this model can be translated to the effect on senile plaques in AD. For example, antibodies targeting truncated Aβ species could result in a false-negative conclusion when using the tgAPPPS1-21 model (<10-month old). Aducanumab was reported to interact with AA sequence 3-6 of Aβ. The level of full-length Aβ (Aβ1-42) was abundant in both tgAPPPS1-21 mice and AD

and the action of aducanumab was therefore considered to be effective in both. Although not the scope of this thesis, we consider that the action of aducanumab could be limited by possibly excluding pyro-glu modified Aβ and truncated Aβ in AD.

Our histological examination of senile plaque load in tgAPPPS1-21 mice treated with aducanumab demonstrated significant clearance in the hippocampus compared to control. The clearance mechanism by aducanumab has been reported to occur via glia cell recruitment (Sevigny et al., 2016). To capture this event, we microdissected senile plaques and surrounding penumbra. Our proteomic analysis of SP extracts suggested a degree of similarity between the treatment groups by having several shared proteins with limited differences in intensity levels after LFQ. In contrast, notable differences were observed across SPP-L1 and SPP-L2 subregions in the three groups, as we identified 18 and 15 significantly differentiating proteins, respectively. Furthermore, several proteins associated with energy metabolism were increased in the aducanumab treated mice. This finding was in line with our hypothesis, as we anticipated the engagement of aducanumab would cause recruitment of glia cells that subsequently would initiate phagocytosis and increase their energy metabolism. We observed increased levels of the astrocytic marker, GFAP, in the SPP-L1 region of aducanumab treated mice compared to IgG which supported this. Furthermore, we identified increased levels of proteins associated with phagocytosis like plastin-2 (LCP1) and phosphatidylinositol 4-phosphate 5-kinase type-1 gamma (PIP5K1C) in the SPP-L1 region when comparing aducanumab to IgG treated mice (1.79-fold, $p = 0.097$; 2.03-fold, $p = 0.067$; LCP1 and PIP5K1C, respectively; student t-test, 0.1 FDR) (Kwiatkowska & Sobota, 1999; Morley, 2012). Our findings from publication II indicated increased levels of proteins associated with endocytosis and energy metabolism when comparing senile plaques to surrounding tissue. This finding was also supported by the data in manuscript III which indicated that these pathways and especially proteins associated with energy metabolism were detected in senile plaques and closely surrounding regions.

Our anticipation of glia recruitment by aducanumab was based on microproteomic data and we consider that validating this finding with other techniques such as immunohistochemistry would be beneficial. It was reported that the level of the

lysosomal marker, CD68, correlated with Aβ1-42 load in patients from the active vaccine (AN-1792) program (See section, **Treatment strategies targeting amyloid-β**) (Zotova et al., 2011). Zotova and colleagues observed co-localization of CD68 and microglia and suggested that a subgroup of microglia were recruited to senile plaques to initiate phagocytosis (Zotova et al., 2011). Additionally, the authors reported differences in microglia activity depending on the Aβ pathology (high plaque load resulted in increased levels of CD68+ microglia while low plaque load resulted in decreased levels of CD68+ microglia). We consider that such cellular subpopulation would be interesting to target in the aducanumab treated tgAPPPPS1-21 mice from our study, as they could represent the proteomic profile that we detected. We identified two GTPase regulating proteins which intensity levels were altered specifically by the aducanumab treatment. Phagocytosis and associated degradation of material is regulated by several GTPases (Mao & Finnemann, 2015; Yeo, Wall, Luo, & Stow, 2016). GTPase regulating proteins are therefore considered highly relevant in respect to clearance of senile plaques. NME1 was observed to be reduced in all subregions from aducanumab compared to controls and did not differentiate as seen in the control groups. In contrast, SDCBP was regulated by aducanumab and observed to be abundant in SP extracts. Our data could therefore suggest that part of the clearance mechanism of aducanumab could be caused by recruitment of a specific subtype of glia cells that host these protein patterns. Different clearance mechanisms have been hypothesized by anti-Aβ targeting antibodies. Our data support a central clearance mechanism by aducanumab that is mediated by glia recruitment to the penumbral region of senile plaques to elicit its effect.

CHAPTER 5. CONCLUSIONS

The presented dissertation has focused on determining different layers of molecular complexity that are associated with senile plaques in both AD and tgAPPPS1-21 model mice.

We reported a parallel approach by combining microdissection and MALDI-MS imaging to overcome issues related to signal suppression hampering the detection of Aβ proteoforms. Additionally, we demonstrated that the use of PA as matrix additive to the sDHB matrix improved the detection of Aβ peptides in MALDI-MS imaging. Using this approach, we identified a central difference in the senile plaque (Aβ-associated) composition between AD and 9-month old tgAPPPS1-21 mice. We report that senile plaques from AD patients are composed of more truncated and modified Aβ proteoforms compared to tgAPPPS1-21 mice.

We reported a microproteomic strategy that enabled isolation and determination of the proteomic profile of senile plaques and surrounding tissue in tgAPPPS1-21 mice. We identified several differentiating proteins that demonstrated regulatory processes associated with endocytosis and metabolism within senile plaque extracts. Furthermore, several exclusive PTMs such as oxidation, deamidation and pyro-glu were identified on the proteins co-localizing with senile plaque extracts in the tgAPPPS1-21 mouse model. Using ProExM, we observed co-aggregation of PGK1 which was identified by our microproteomic approach.

We found that chronic treatment with the anti-Aβ targeting antibody, aducanumab, significantly reduced the senile plaque load in hippocampus compared to the control groups. Using the MS-based strategies, we demonstrated that the proteomic complexity of the closely located penumbral region of senile plaques was affected by the treatment. Our data supported that the clearance mechanism by aducanumab occurred via glia cell recruitment and possibly through increased energy metabolism and modulation of GTPase regulating proteins that are involved in phagocytosis.

We believe that our findings have clarified part of the molecular complexity associated with senile plaques in the tgAPPPS1-21 mouse model. Our data has contributed to a general understanding of molecular processes occurring in senile

plaques, closely surrounding tissue and how it is affected by an anti-Aβ targeting antibody. The identification of regulated proteins and PTMs could lead to novel drug types that modulate phagocytic clearance of Aβ in AD.

CHAPTER 6. PERSPECTIVES

The results presented in this dissertation suggest that several proteins including their modified forms are co-localizing and/or co-aggregating with aggregated Aβ. It is essential to elucidate the biological function of these proteins and PTMs as they could have a beneficial or detrimental impact on disease pathogenesis and future studies should therefore investigate these mechanisms. Three-dimensional neuronal co-cultures consisting of human cell types expressing FAD mutations are suggested as a simple and relative fast method to answer these questions (Choi et al., 2014). Such a method would allow establishment of a platform that could be used to both visualize the many proteins e.g. with microscopy and screen the effect of compounds that specifically target these proteins. The knowledge, and ideally new targets uncovered from such experiments could be used in combination with current antibody therapies to boost the treatment effect or overcome the weaknesses of current antibody therapies. It is noteworthy that a high load of senile plaques was still present in both gantenerumab and aducanumab mice after chronic treatment. This may suggest that these antibodies are not capable of removing all senile plaques or that the kinetics of plaque clearance in AD cannot be adequately modeled in tg mice. It is considered that finding alternative approaches to reach these subtypes of senile plaques could optimize clearing efficiency.

Both MALDI-MS imaging and microproteomics are relatively young scientific fields that have challenges which future studies should address. For example, sensitivity issues in MALDI-MS imaging are currently a major limitation that hampers the outcome. We addressed this issue in (publication I), but it is considered that further optimization of the method would be beneficial. A recent advancement of MALDI-MS imaging, termed MALDI-2, argues that the low sensitivity is a consequence of poor ionization and reports the use of a secondary post-ionization process increases the sensitivity several orders of magnitude (Soltwisch et al., 2015). Similarly, microproteomic suffers from limited sample material and approaches that can ensure the maximum yield of each sample are highly valued. For example, DIA-based

methods such as DIA-PASEF could maximize the sample coverage and identification rate if a proper fragmentation library was established (Gillet et al., 2012).

CHAPTER 7. REFERENCES

Adav, S. S., Gallart-Palau, X., Tan, K. H., Lim, S. K., Tam, J. P., & Sze, S. K. (2016). Dementia-linked amyloidosis is associated with brain protein deamidation as revealed by proteomic profiling of human brain tissues. *Molecular Brain*, *9*(1), 20. https://doi.org/10.1186/s13041-016-0200-z

Aebersold, R., & Mann, M. (2016). Mass-spectrometric exploration of proteome structure and function. *Nature*, *537*(7620), 347–355. https://doi.org/10.1038/nature19949

Akiyama, H., Mori, H., Saido, T., Kondo, H., Ikeda, K., & McGeer, P. L. (1999). Occurrence of the diffuse amyloid β-protein (Aβ) deposits with numerous Aβ-containing glial cells in the cerebral cortex of patients with Alzheimer's disease. *Glia*, *25*(4), 324–331. https://doi.org/10.1002/(SICI)1098-1136(19990215)25:4<324::AID-GLIA2>3.0.CO;2-5

Annaert, W., & De Strooper, B. (2002). A Cell Biological Perspective on Alzheimer's Disease. *Annual Review of Cell and Developmental Biology*, *18*(1), 25–51. https://doi.org/10.1146/annurev.cellbio.18.020402.142302

Atwood, C. S., Martins, R. N., Smith, M. A., & Perry, G. (2002). Senile plaque composition and posttranslational modification of amyloid-β peptide and associated proteins. *Peptides*, *23*(7), 1343–1350. https://doi.org/10.1016/S0196-9781(02)00070-0

Barrow, C., & Zagorski, M. (1991). Solution structures of beta peptide and its constituent fragments: relation to amyloid deposition. *Science*, *253*(5016), 179–182. https://doi.org/10.1126/science.1853202

Bateman, R. J., Aisen, P. S., De Strooper, B., Fox, N. C., Lemere, C. A., Ringman, J. M., … Xiong, C. (2010). Autosomal-dominant Alzheimer's disease: a review and proposal for the prevention of Alzheimer's disease. *Alzheimer's Research & Therapy*, *3*(1), 1. https://doi.org/10.1186/alzrt59

Beavis, R. C., Chaudhary, T., & Chait, B. T. (1992). α-Cyano-4-hydroxycinnamic acid as a matrix for matrixassisted laser desorption mass spectromtry. *Organic Mass Spectrometry*, *27*(2), 156–158. https://doi.org/10.1002/oms.1210270217

Beavis, Ronald C., Chait, B. T., & Standing, K. G. (1989). Matrix-assisted laser-desorption mass spectrometry using 355 nm radiation. *Rapid Communications in Mass Spectrometry*, *3*(12), 436–439. https://doi.org/10.1002/rcm.1290031208

Bennike, T. B., Kastaniegaard, K., Padurariu, S., Gaihede, M., Birkelund, S., Andersen, V., & Stensballe, A. (2016). Comparing the proteome of snap frozen, RNAlater preserved, and formalin-fixed paraffin-embedded human tissue samples. *EuPA Open Proteomics*, *10*, 9–18. https://doi.org/10.1016/j.euprot.2015.10.001

Bittner, T., Burgold, S., Dorostkar, M. M., Fuhrmann, M., Wegenast-braun, B., Schmidt, B., & Herms, J. (2012). Amyloid plaque formation precedes dendritic spine loss. *Acta Neuropathologica*, *124*(6), 797–807. https://doi.org/10.1007/s00401-012-1047-8

Blazquez-Llorca, L., Merchán-Pérez, Á., Rodríguez, J.-R., Gascón, J., & DeFelipe, J. (2013). FIB/SEM Technology and Alzheimer's Disease: Three-Dimensional Analysis of Human Cortical Synapses. *Journal of Alzheimer's Disease*, *34*(4), 995–1013. https://doi.org/10.3233/JAD-122038

Bohrmann, B., & Baumann, K. (2012). Gantenerumab: A Novel Human Anti-Aβ Antibody Demonstrates Sustained Cerebral Amyloid-β Binding and Elicits Cell-Mediated Removal of Human. *Journal of Alzheimer's Disease*, *28*(1), 49–69. https://doi.org/10.3233/JAD-2011-110977

Braak, H., & Braak, E. (1991). Neuropathological stageing of Alzheimer-related changes. *Acta Neuropathologica*, *82*(4), 239–259. https://doi.org/10.1007/BF00308809

Brookmeyer, R., Corrada, M. M., Curriero, F. C., & Kawas, C. (2002). Survival Following a Diagnosis of Alzheimer Disease. *Archives of Neurology*, *59*(11), 1764–1767. https://doi.org/10.1001/archneur.59.11.1764

Bussière, T., Bard, F., Barbour, R., Grajeda, H., Guido, T., Khan, K., … Buttini, M. (2004). Morphological Characterization of Thioflavin-S-Positive Amyloid Plaques in Transgenic Alzheimer Mice and Effect of Passive Aβ Immunotherapy on Their Clearance. *The American Journal of Pathology*, *165*(3), 987–995. https://doi.org/10.1016/S0002-9440(10)63360-3

Cai, R., Zhang, Y., Simmering, J. E., Schultz, J. L., Li, Y., Fernandez-Carasa, I., … Liu, L. (2019). Enhancing glycolysis attenuates Parkinson's disease progression in models and clinical databases. *Journal of Clinical Investigation*, *129*(10), 4539–4549. https://doi.org/10.1172/JCI129987

Caprioli, R. M., Farmer, T. B., & Gile, J. (1997). Molecular Imaging of Biological Samples: Localization of Peptides and Proteins Using MALDI-TOF MS. *Analytical Chemistry*, *69*(23), 4751–4760. https://doi.org/10.1021/ac970888i

Carlred, L., Michno, W., Kaya, I., Sjövall, P., Syvänen, S., & Hanrieder, J. (2016). Probing amyloid-β pathology in transgenic Alzheimer's disease (tgArcSwe) mice using MALDI imaging mass spectrometry. *Journal of Neurochemistry*, *138*(3), 469–478. https://doi.org/10.1111/jnc.13645

Cataldo, A. M., Thayer, C. Y., Bird, E. D., Wheelock, T. R., & Nixon, R. A. (1990). Lysosomal proteinase antigens are prominently localized within senile plaques of Alzheimer's disease: evidence for a neuronal origin. *Brain Research*, *513*(2), 181–192. https://doi.org/10.1016/0006-8993(90)90456-L

Chartier-Harlin, M.-C., Crawford, F., Houlden, H., Warren, A., Hughes, D., Fidani, L., … Mullan, M. (1991). Early-onset Alzheimer's disease caused by mutations at codon 717 of the β-amyloid precursor protein gene. *Nature*, *353*(6347), 844–846. https://doi.org/10.1038/353844a0

Chen, F., Tillberg, P. W., & Boyden, E. S. (2015). Expansion microscopy. *Science*, *347*(6221), 543–548. https://doi.org/10.1126/science.1260088

Choi, S. H., Kim, Y. H., Hebisch, M., Sliwinski, C., Lee, S., D'Avanzo, C., … Kim, D. Y. (2014). A three-dimensional human neural cell culture model of Alzheimer's disease. *Nature*, *515*(7526), 274–278. https://doi.org/10.1038/nature13800

Choudhary, C., & Mann, M. (2010). Decoding signalling networks by mass spectrometry-based proteomics. *Nature Reviews Molecular Cell Biology*, *11*(6), 427–439. https://doi.org/10.1038/nrm2900

De Marchi, T., Braakman, R. B. H., Stingl, C., van Duijn, M. M., Smid, M., Foekens, J. A., … Umar, A. (2016). The advantage of laser-capture microdissection over whole tissue analysis in proteomic profiling studies. *PROTEOMICS*, *16*(10), 1474–1485. https://doi.org/10.1002/pmic.201600004

De Rossi, P., Andrew, R. J., Musial, T. F., Buggia-Prevot, V., Xu, G., Ponnusamy, M., … Thinakaran, G. (2019). Aberrant accrual of BIN1 near Alzheimer's disease amyloid deposits in transgenic models. *Brain Pathology*, *29*(4), 485–501. https://doi.org/10.1111/bpa.12687

DeTure, M. A., & Dickson, D. W. (2019). The neuropathological diagnosis of Alzheimer's disease. *Molecular Neurodegeneration*, *14*(1), 32. https://doi.org/10.1186/s13024-019-0333-5

Drummond, E., Nayak, S., Faustin, A., Pires, G., Hickman, R. A., Askenazi, M., … Safar, J. G. (2017). Proteomic differences in amyloid plaques in rapidly progressive and sporadic Alzheimer's disease. *Acta Neuropathologica*, *133*(6),

933–954. https://doi.org/10.1007/s00401-017-1691-0

Drummond, E., & Wisniewski, T. (2017). Alzheimer's disease: experimental models and reality. *Acta Neuropathologica*, *133*(2), 155–175. https://doi.org/10.1007/s00401-016-1662-x

Eng, J. K., McCormack, A. L., & Yates, J. R. (1994). An approach to correlate tandem mass spectral data of peptides with amino acid sequences in a protein database. *Journal of the American Society for Mass Spectrometry*, *5*(11), 976–989. https://doi.org/10.1016/1044-0305(94)80016-2

Fan, Z., Brooks, D. J., Okello, A., & Edison, P. (2017). An early and late peak in microglial activation in Alzheimer's disease trajectory. *Brain*, *140*(3), 792–803. https://doi.org/10.1093/brain/aww349

Förstl, H., & Kurz, A. (1999). Clinical features of Alzheimer's disease. *European Archives of Psychiatry and Clinical Neuroscience*, *249*(6), 288–290. https://doi.org/10.1007/s004060050101

Furukawa, K., Sopher, B. L., Rydel, R. E., Begley, J. G., Pham, D. G., Martin, G. M., … Mattson, M. P. (2002). Increased Activity-Regulating and Neuroprotective Efficacy of α-Secretase-Derived Secreted Amyloid Precursor Protein Conferred by a C-Terminal Heparin-Binding Domain. *Journal of Neurochemistry*, *67*(5), 1882–1896. https://doi.org/10.1046/j.1471-4159.1996.67051882.x

Gemperline, E., Rawson, S., & Li, L. (2014). Optimization and Comparison of Multiple MALDI Matrix Application Methods for Small Molecule Mass Spectrometric Imaging. *Analytical Chemistry*, *86*(20), 10030–10035. https://doi.org/10.1021/ac5028534

Gillet, L. C., Navarro, P., Tate, S., Röst, H., Selevsek, N., Reiter, L., … Aebersold, R. (2012). Targeted Data Extraction of the MS/MS Spectra Generated by Data-independent Acquisition: A New Concept for Consistent and Accurate Proteome Analysis. *Molecular & Cellular Proteomics*, *11*(6), O111.016717. https://doi.org/10.1074/mcp.O111.016717

Godyń, J., Jończyk, J., Panek, D., & Malawska, B. (2016). Therapeutic strategies for Alzheimer's disease in clinical trials. *Pharmacological Reports*, *68*(1), 127–138. https://doi.org/10.1016/j.pharep.2015.07.006

Goedert, M., Spillantini, M. G., Cairns, N. J., & Crowther, R. A. (1992). Tau proteins of alzheimer paired helical filaments: Abnormal phosphorylation of all six brain isoforms. *Neuron*, *8*(1), 159–168. https://doi.org/10.1016/0896-6273(92)90117-V

Goedert, M., Spillantini, M. G., & Crowther, R. A. (1991). Tau Proteins and Neurofibrillary Degeneration. *Brain Pathology*, *1*(4), 279–286. https://doi.org/10.1111/j.1750-3639.1991.tb00671.x

Goedert, M., Spillantini, M. G., Potier, M. C., Ulrich, J., & Crowther, R. A. (1989). Cloning and sequencing of the cDNA encoding an isoform of microtubule-associated protein tau containing four tandem repeats: differential expression of tau protein mRNAs in human brain. *The EMBO Journal*, *8*(2), 393–399. https://doi.org/10.1002/j.1460-2075.1989.tb03390.x

Güntert, A., Döbeli, H., & Bohrmann, B. (2006). High sensitivity analysis of amyloid-beta peptide composition in amyloid deposits from human and PS2APP mouse brain. *Neuroscience*, *143*(2), 461–475. https://doi.org/10.1016/j.neuroscience.2006.08.027

Han, Xi, He, L., Xin, L., Shan, B., & Ma, B. (2011). PeaksPTM: Mass spectrometry-based identification of peptides with unspecified modifications. *Journal of Proteome Research*, *10*(7), 2930–2936. https://doi.org/10.1021/pr200153k

Han, Xuemei, Aslanian, A., & Yates, J. R. (2008). Mass spectrometry for proteomics. *Current Opinion in Chemical Biology*, *12*(5), 483–490. https://doi.org/10.1016/j.cbpa.2008.07.024

Hardy, J., & Selkoe, D. J. (2002). The Amyloid Hypothesis of Alzheimer's Disease: Progress and Problems on the Road to Therapeutics. *Science*, *297*(5580), 353–356. https://doi.org/10.1126/science.1072994

Heneka, M. T., Carson, M. J., Khoury, J. El, Landreth, G. E., Brosseron, F., Feinstein, D. L., … Kummer, M. P. (2015). Neuroinflammation in Alzheimer's disease. *The Lancet Neurology*, *14*(4), 388–405. https://doi.org/10.1016/S1474-4422(15)70016-5

Hensley, K., Hall, N., Subramaniam, R., Cole, P., Harris, M., Aksenov, M., … Butterfield, D. A. (1995). Brain Regional Correspondence Between Alzheimer's Disease Histopathology and Biomarkers of Protein Oxidation. *Journal of Neurochemistry*, *65*(5), 2146–2156. https://doi.org/10.1046/j.1471-4159.1995.65052146.x

Ho, C. S., Lam, C. W. K., Chan, M. H. M., Cheung, R. C. K., Law, L. K., Lit, L. C. W., … Tai, H. L. (2003). Electrospray ionisation mass spectrometry: principles and clinical applications. *The Clinical Biochemist. Reviews*, *24*(1), 3–12. https://doi.org/10.1002/9781118307816.ch34

Ho Kim, J., Franck, J., Kang, T., Heinsen, H., Ravid, R., Ferrer, I., … Mok Park, Y.

(2015). Proteome-wide characterization of signalling interactions in the hippocampal CA4/DG subfield of patients with Alzheimer's disease. *Scientific Reports*, *5*(1), 11138. https://doi.org/10.1038/srep11138

Hsiao, K., Chapman, P., Nilsen, S., Eckman, C., Harigaya, Y., Younkin, S., … Cole, G. (1996). Correlative Memory Deficits, Aβ Elevation, and Amyloid Plaques in Transgenic Mice. *Science*, *274*(5284), 99–103. https://doi.org/10.1126/science.274.5284.99

Ikegawa, M., Nirasawa, T., Kakuda, N., Miyasaka, T., Kuzuhara, Y., Murayama, S., & Ihara, Y. (2019). Visualization of Amyloid β Deposits in the Human Brain with Matrix-assisted Laser Desorption/Ionization Imaging Mass Spectrometry. *Journal of Visualized Experiments*, *145*, e57645. https://doi.org/10.3791/57645

Ishigami, A., Ohsawa, T., Hiratsuka, M., Taguchi, H., Kobayashi, S., Saito, Y., … Maruyama, N. (2005). Abnormal accumulation of citrullinated proteins catalyzed by peptidylarginine deiminase in hippocampal extracts from patients with Alzheimer's disease. *Journal of Neuroscience Research*, *80*(1), 120–128. https://doi.org/10.1002/jnr.20431

Jack, C. J., Knopman, D. S., Jagust, W. J., Shaw, L. M., Aisen, P. S., Weiner, M. W., … Trojanowski, J. Q. (2010). Hypothetical model of dynamic biomarkers of the Alzheimer's pathological cascade. *Lancet Neurol.*, *9*(1), 119–128. https://doi.org/10.1016/S1474-4422(09)70299-6

Jacobsen, H., Ozmen, L., Caruso, A., Narquizian, R., Hilpert, H., Jacobsen, B., … Bohrmann, B. (2014). Combined Treatment with a BACE Inhibitor and Anti-Aβ Antibody Gantenerumab Enhances Amyloid Reduction in APPLondon Mice. *Journal of Neuroscience*, *34*(35), 11621–11630. https://doi.org/10.1523/JNEUROSCI.1405-14.2014

Jansen, I. E., Savage, J. E., Watanabe, K., Bryois, J., Williams, D. M., Steinberg, S., … Posthuma, D. (2019). Genome-wide meta-analysis identifies new loci and functional pathways influencing Alzheimer's disease risk. *Nature Genetics*, *51*(3), 404–413. https://doi.org/10.1038/s41588-018-0311-9

Jawhar, S., Wirths, O., & Bayer, T. A. (2011). Pyroglutamate amyloid-β (Aβ): a hatchet man in Alzheimer disease. *Journal of Biological Chemistry*, *286*(45), 38825–38832. https://doi.org/10.1074/jbc.R111.288308

Jensen, O. (2004). Modification-specific proteomics: characterization of post-translational modifications by mass spectrometry. *Current Opinion in Chemical Biology*, *8*(1), 33–41. https://doi.org/10.1016/j.cbpa.2003.12.009

Jin, M., Shepardson, N., Yang, T., Chen, G., Walsh, D., & Selkoe, D. J. (2011). Soluble amyloid β-protein dimers isolated from Alzheimer cortex directly induce Tau hyperphosphorylation and neuritic degeneration. *Proceedings of the National Academy of Sciences*, *108*(14), 5819–5824. https://doi.org/10.1073/pnas.1017033108

Johnson, E. C. B., Dammer, E. B., Duong, D. M., Yin, L., Thambisetty, M., Troncoso, J. C., … Seyfried, N. T. (2018). Deep proteomic network analysis of Alzheimer's disease brain reveals alterations in RNA binding proteins and RNA splicing associated with disease. *Molecular Neurodegeneration*, *13*(1), 52. https://doi.org/10.1186/s13024-018-0282-4

Kakuda, N., Miyasaka, T., Iwasaki, N., Nirasawa, T., & Wada-kakuda, S. (2017). Distinct deposition of amyloid-β species in brains with Alzheimer's disease pathology visualized with MALDI imaging mass spectrometry. *Acta Neuropathologica Communications*, *5*(73), 1–8. https://doi.org/10.1186/s40478-017-0477-x

Karas, M., Bachmann, D., & Hillenkamp, F. (1985). Influence of the Wavelength in High-Irradiance Ultraviolet Laser Desorption Mass Spectrometry of Organic Molecules. *Analytical Chemistry*, *57*(14), 2935–2939. https://doi.org/10.1021/ac00291a042

Karas, M., & Hillenkamp, F. (1988). Laser desorption ionization of proteins with molecular masses exceeding 10,000 daltons. *Analytical Chemistry*, *60*(20), 2299–2301. https://doi.org/10.1021/ac00171a028

Kaya, I., Brinet, D., Michno, W., Syvänen, S., Sehlin, D., Zetterberg, H., … Hanrieder, J. (2017). Delineating Amyloid Plaque Associated Neuronal Sphingolipids in Transgenic Alzheimer's Disease Mice (tgArcSwe) Using MALDI Imaging Mass Spectrometry. *ACS Chemical Neuroscience*, *8*(2), 347–355. https://doi.org/10.1021/acschemneuro.6b00391

Kaya, I., Brinet, D., Michno, W., Zetterberg, H., & Blenow, K. (2017). Novel Trimodal MALDI Imaging Mass Spectrometry (IMS3) at 10 μm Reveals Spatial Lipid and Peptide Correlates Implicated in Aβ Plaque Pathology in Alzheimer 's Disease. *ACS Chem. Neurosci*, *8*(12), 2778–2790. https://doi.org/10.1021/acschemneuro.7b00314

Kaya, I., Michno, W., Brinet, D., Iacone, Y., Zanni, G., Blennow, K., … Hanrieder, J. (2017). Histology-Compatible MALDI Mass Spectrometry Based Imaging of Neuronal Lipids for Subsequent Immunofluorescent Staining. *Analytical Chemistry*, *89*(8), 4685–4694. https://doi.org/10.1021/acs.analchem.7b00313

Kaya, I., Zetterberg, H., Blennow, K., & Hanrieder, J. (2018). Shedding Light on the Molecular Pathology of Amyloid Plaques in Transgenic Alzheimer's Disease Mice Using Multimodal MALDI Imaging Mass Spectrometry. *ACS Chemical Neuroscience*, *9*(7), 1802–1817. https://doi.org/10.1021/acschemneuro.8b00121

Kelley, A. R., Perry, G., Bethea, C., Castellani, R. J., & Bach, S. B. H. (2016). Molecular Mapping Alzheimer's Disease: MALDI Imaging of Formalin-fixed, Paraffin-embedded Human Hippocampal Tissue. *The Open Neurology Journal*, *10*(1), 88–98. https://doi.org/10.2174/1874205X01610010088

Kelley, A. R., Perry, G., Castellani, R. J., & Bach, S. B. H. (2016). Laser-Induced In-Source Decay Applied to the Determination of Amyloid-Beta in Alzheimer's Brains. *ACS Chemical Neuroscience*, *7*(3), 261–268. https://doi.org/10.1021/acschemneuro.5b00295

Kim, J., & Dang, C. V. (2005). Multifaceted roles of glycolytic enzymes. *Trends in Biochemical Sciences*, *30*(3), 142–150. https://doi.org/10.1016/j.tibs.2005.01.005

Kjellstrtöm, S., & Jensen, O. N. (2004). Phosphoric acid as a matrix additive for MALDI MS analysis of phosphopeptides and phosphoproteins. *Analytical Chemistry*, *76*(17), 5109–5117. https://doi.org/10.1021/ac0400257

Klunk, W. E., Engler, H., Nordberg, A., Wang, Y., Blomqvist, G., Holt, D. P., … Långström, B. (2004). Imaging brain amyloid in Alzheimer's disease with Pittsburgh Compound-B. *Annals of Neurology*, *55*(3), 306–319. https://doi.org/10.1002/ana.20009

Koistinaho, M., Lin, S., Wu, X., Esterman, M., Koger, D., Hanson, J., … Paul, S. M. (2004). Apolipoprotein E promotes astrocyte colocalization and degradation of deposited amyloid-β peptides. *Nature Medicine*, *10*(7), 719–726. https://doi.org/10.1038/nm1058

Kummer, M. P., & Heneka, M. T. (2014). Truncated and modified amyloid-beta species. *Alzheimer's Research & Therapy*, *6*(28), 1–9. https://doi.org/10.1186/alzrt258

Kuyama, H., Sonomura, K., & Nishimura, O. (2008). Sensitive detection of phosphopeptides by matrix-assisted laser desorption/ionization mass spectrometry: use of alkylphosphonic acids as matrix additives. *Rapid Communications in Mass Spectrometry*, *22*(8), 1109–1116. https://doi.org/10.1002/rcm.3482

Kwiatkowska, K., & Sobota, A. (1999). Signaling pathways in phagocytosis. *BioEssays*, *21*(5), 422–431. https://doi.org/10.1002/(SICI)1521-1878(199905)21:5<422::AID-BIES9>3.0.CO;2-%23

Lambert, J.-C., Ibrahim-Verbaas, C. A., Harold, D., Naj, A. C., Sims, R., Bellenguez, C., … Amouyel, P. (2013). Meta-analysis of 74,046 individuals identifies 11 new susceptibility loci for Alzheimer's disease. *Nature Genetics*, *45*(12), 1452–1458. https://doi.org/10.1038/ng.2802

Laugesen, S., & Roepstorff, P. (2003). Combination of Two Matrices Results in Improved Performance of MALDI MS for Peptide Mass Mapping and Protein Analysis. *Am Soc Mass Spectrom*, *14*(9), 992–1002. https://doi.org/10.1016/S1044-0305(03)00262-9

Liao, L., Cheng, D., Wang, J., Duong, D. M., Losik, T. G., Gearing, M., … Peng, J. (2004). Proteomic Characterization of Postmortem Amyloid Plaques Isolated by Laser Capture Microdissection. *Journal of Biological Chemistry*, *279*(35), 37061–37068. https://doi.org/10.1074/jbc.M403672200

Liu, K., Solano, I., Mann, D., Lemere, C., Mercken, M., Trojanowski, J. Q., & Lee, V. M. (2006). Characterization of Aβ11-40/42 peptide deposition in Alzheimer's disease and young Down's syndrome brains: implication of N-terminally truncated Aβ species in the pathogenesis of Alzheimer's disease. *Acta Neuropathologica*, *112*(2), 163–174. https://doi.org/10.1007/s00401-006-0077-5

Lord, A., Kalimo, H., Eckman, C., Zhang, X.-Q., Lannfelt, L., & Nilsson, L. N. G. (2006). The Arctic Alzheimer mutation facilitates early intraneuronal Aβ aggregation and senile plaque formation in transgenic mice. *Neurobiology of Aging*, *27*(1), 67–77. https://doi.org/10.1016/j.neurobiolaging.2004.12.007

Lutz, B., & Peng, J. (2018). Deep Profiling of the Aggregated Proteome in Alzheimer's Disease: From Pathology to Disease Mechanisms. *Proteomes*, *6*(4), 46. https://doi.org/10.3390/proteomes6040046

Mao, Y., & Finnemann, S. C. (2015). Regulation of phagocytosis by Rho GTPases. *Small GTPases*, *6*(2), 89–99. https://doi.org/10.4161/21541248.2014.989785

Masters, C. L., Simms, G., Weinman, N. A., Multhaupt, G., & Mcdonald, B. L. (1985). Amyloid plaque core protein in Alzheimer disease and Down syndrome. *Proc. Natl. Acad. Sci. USA*, *82*(12), 4245–4249. https://doi.org/10.1073/pnas.82.12.4245

Meier, F., Brunner, A.-D., Koch, S., Koch, H., Lubeck, M., Krause, M., … Mann, M.

(2018). Online Parallel Accumulation–Serial Fragmentation (PASEF) with a Novel Trapped Ion Mobility Mass Spectrometer. *Molecular & Cellular Proteomics*, *17*(12), 2534–2545. https://doi.org/10.1074/mcp.TIR118.000900

Meldolesi, J. (2018). Exosomes and Ectosomes in Intercellular Communication. *Current Biology*, *28*(8), R435–R444. https://doi.org/10.1016/j.cub.2018.01.059

Mendis, L. H. S., Grey, A. C., Faull, R. L. M., & Curtis, M. A. (2016). Hippocampal lipid differences in Alzheimer's disease: a human brain study using matrix-assisted laser desorption/ionization-imaging mass spectrometry. *Brain and Behavior*, *6*(10), e00517. https://doi.org/10.1002/brb3.517

Michno, W., Kaya, I., Nyström, S., Guerard, L., Nilsson, K. P. R., Hammarström, P., … Hanrieder, J. (2018). Multimodal Chemical Imaging of Amyloid Plaque Polymorphism Reveals Aβ Aggregation Dependent Anionic Lipid Accumulations and Metabolism. *Analytical Chemistry*, *90*(13), 8130–8138. https://doi.org/10.1021/acs.analchem.8b01361

Michno, W., Wehrli, P. M., Zetterberg, H., Blennow, K., & Hanrieder, J. (2019). GM1 locates to mature amyloid structures implicating a prominent role for glycolipid-protein interactions in Alzheimer pathology. *Biochimica et Biophysica Acta (BBA) - Proteins and Proteomics*, *1867*(5), 458–467. https://doi.org/10.1016/j.bbapap.2018.09.010

Mlodzianoski, M., Cheng-Hathaway, P., Liu, S., Bemiller, S., McCray, T., Miller, D., … Huang, F. (2019). Active PSF Shaping and Adaptive Optics Enable Volumetric Single Molecule Super-Resolution Microscopy through Brain Sections. *Biophysical Journal*, *116*(3), 283a-284a. https://doi.org/10.1016/j.bpj.2018.11.1533

Morley, S. C. (2012). The Actin-Bundling Protein L-Plastin: A Critical Regulator of Immune Cell Function. *International Journal of Cell Biology*, *2012*, 1–10. https://doi.org/10.1155/2012/935173

Moro, M. L., Phillips, A. S., Gaimster, K., Paul, C., Mudher, A., Nicoll, J. A. R., & Boche, D. (2018). Pyroglutamate and Isoaspartate modified Amyloid-Beta in ageing and Alzheimer's disease. *Acta Neuropathologica Communications*, *6*(1), 3. https://doi.org/10.1186/s40478-017-0505-x

Mucke, L., Masliah, E., Yu, G.-Q., Mallory, M., Rockenstein, E. M., Tatsuno, G., … McConlogue, L. (2000). High-Level Neuronal Expression of Aβ 1–42 in Wild-Type Human Amyloid Protein Precursor Transgenic Mice: Synaptotoxicity without Plaque Formation. *The Journal of Neuroscience*, *20*(11), 4050–4058. https://doi.org/10.1523/JNEUROSCI.20-11-04050.2000

Nasiri Kenari, A., Kastaniegaard, K., Greening, D. W., Shambrook, M., Stensballe, A., Cheng, L., & Hill, A. F. (2019). Proteomic and Post-Translational Modification Profiling of Exosome-Mimetic Nanovesicles Compared to Exosomes. *PROTEOMICS*, *19*(8), 1800161. https://doi.org/10.1002/pmic.201800161

Nelson, P. T., Braak, H., & Markesbery, W. R. (2009). Neuropathology and Cognitive Impairment in Alzheimer Disease: A Complex but Coherent Relationship. *Journal of Neuropathology & Experimental Neurology*, *68*(1), 1–14. https://doi.org/10.1097/NEN.0b013e3181919a48

Nicoll, J. A. R., Wilkinson, D., Holmes, C., Steart, P., Markham, H., & Weller, R. O. (2003). Neuropathology of human Alzheimer disease after immunization with amyloid-β peptide: a case report. *Nature Medicine*, *9*(4), 448–452. https://doi.org/10.1038/nm840

Norris, J. L., & Caprioli, R. M. (2013). Analysis of tissue specimens by matrix-assisted laser desorption/ionization imaging mass spectrometry in biological and clinical research. *Chemical Reviews*, *113*(4), 2309–2342. https://doi.org/10.1021/cr3004295

Oda, T., Wals, P., Osterburg, H. H., Johnson, S. A., Pasinetti, G. M., Morgan, T. E., … Finch, C. E. (1995). Clusterin (apoJ) Alters the Aggregation of Amyloid β-Peptide (Aβ1-42) and Forms Slowly Sedimenting Aβ Complexes That Cause Oxidative Stress. *Experimental Neurology*, *136*(1), 22–31. https://doi.org/10.1006/exnr.1995.1080

Ostrowitzki, S., Deptula, D., Thurfjell, L., Barkhof, F., Bohrmann, B., Brooks, D. J., … Santarelli, L. (2012). Mechanism of Amyloid Removal in Patients With Alzheimer Disease Treated With Gantenerumab. *Archives of Neurology*, *69*(2), 198–207. https://doi.org/10.1001/archneurol.2011.1538

Panza, F., Lozupone, M., Logroscino, G., & Imbimbo, B. P. (2019). A critical appraisal of amyloid-β-targeting therapies for Alzheimer disease. *Nature Reviews Neurology*, *15*(2), 73–88. https://doi.org/10.1038/s41582-018-0116-6

Park, S., Kim, T., Lee, J., Seo, M., & Kim, J. (2013). Effect of phosphoric acid as a matrix additive in matrix-assisted laser desorption/ionization analysis. *Rapid Communications in Mass Spectrometry*, *27*(7), 842–846. https://doi.org/10.1002/rcm.6508

Piccini, A., Russo, C., Gliozzi, A., Relini, A., Vitali, A., Borghi, R., … Tabaton, M. (2005). β-Amyloid Is Different in Normal Aging and in Alzheimer Disease. *Journal of Biological Chemistry*, *280*(40), 34186–34192.

https://doi.org/10.1074/jbc.M501694200

Pirmoradian, M., Budamgunta, H., Chingin, K., Zhang, B., Astorga-wells, J., & Zubarev, R. A. (2013). Rapid and Deep Human Proteome Analysis by Single-dimension Shotgun Proteomics. *Mol. Cell Proteomics*, *12*(11), 3330–3338. https://doi.org/10.1074/mcp.O113.028787

Prince, M., Wimo, A. G. M., Ali, G.-C., Wu, Y.-T., & Prina, M. (2015). *Alzheimer's Disease International (2015) World Alzheimer Report: The global impact of dementia: an analysis of prevalence, incidence, cost and trends*. Retrieved from https://www.alz.co.uk/research/WorldAlzheimerReport2015.pdf

Probst, A., Brunnschweiler, H., Lautenschlager, C., & Ulrich, J. (1987). A special type of senile plaque, possibly an initial stage. *Acta Neuropathologica*, *74*(2), 133–141. https://doi.org/10.1007/BF00692843

Querol-Vilaseca, M., Colom-Cadena, M., Pegueroles, J., Nuñez-Llaves, R., Luque-Cabecerans, J., Muñoz-Llahuna, L., … Lleó, A. (2019). Nanoscale structure of amyloid-β plaques in Alzheimer's disease. *Scientific Reports*, *9*(1), 5181. https://doi.org/10.1038/s41598-019-41443-3

Radde, R., Bolmont, T., Kaeser, S. A., Coomaraswamy, J., Lindau, D., Stoltze, L., … Jucker, M. (2006). Aβ42-driven cerebral amyloidosis in transgenic mice reveals early and robust pathology. *EMBO Reports*, *7*(9), 940–946. https://doi.org/10.1038/sj.embor.7400784

Richards, J. G., Higgins, G. A., Ouagazzal, A.-M., Ozmen, L., Kew, J. N. C., Bohrmann, B., … Kemp, J. A. (2003). PS2APP Transgenic Mice, Coexpressing hPS2mut and hAPPswe, Show Age-Related Cognitive Deficits Associated with Discrete Brain Amyloid Deposition and Inflammation. *The Journal of Neuroscience*, *23*(26), 8989–9003. https://doi.org/10.1523/JNEUROSCI.23-26-08989.2003

Rogaev, E. I., Sherrington, R., Rogaeva, E. A., Levesque, G., Ikeda, M., Liang, Y., … George-Hyslop, P. H. S. (1995). Familial Alzheimer's disease in kindreds with missense mutations in a gene on chromosome 1 related to the Alzheimer's disease type 3 gene. *Nature*, *376*(6543), 775–778. https://doi.org/10.1038/376775a0

Rohner, T. C., Staab, D., & Stoeckli, M. (2005). MALDI mass spectrometric imaging of biological tissue sections. *Mechanisms of Ageing and Development*, *126*(1), 177–185. https://doi.org/10.1016/j.mad.2004.09.032

Scheltema, R. A., Hauschild, J., Lange, O., Hornburg, D., Denisov, E., Damoc, E., …

Mann, M. (2014). The Q Exactive HF, a Benchtop Mass Spectrometer with a Pre-filter, High-performance Quadrupole and an Ultra-high-field Orbitrap Analyzer. *Molecular & Cellular Proteomics*, *13*(12), 3698–3708. https://doi.org/10.1074/mcp.M114.043489

Schenk, D., Barbour, R., Dunn, W., Gordon, G., Grajeda, H., Guido, T., … Seubert, P. (1999). Immunization with amyloid-β attenuates Alzheimer-disease-like pathology in the PDAPP mouse. *Nature*, *400*(6740), 173–177. https://doi.org/10.1038/22124

Seeley, E. H., & Caprioli, R. M. (2008). Molecular imaging of proteins in tissues by mass spectrometry. *Proceedings of the National Academy of Sciences*, *105*(47), 18126–18131. https://doi.org/10.1073/pnas.0801374105

Selkoe, D. J. (2019). Alzheimer disease and aducanumab: adjusting our approach. *Nature Reviews Neurology*, *15*(7), 365–366. https://doi.org/10.1038/s41582-019-0205-1

Sergeant, N., Bombois, S., Ghestem, A., Drobecq, H., Kostanjevecki, V., Missiaen, C., … Delacourte, A. (2003). Truncated beta-amyloid peptide species in pre-clinical Alzheimer's disease as new targets for the vaccination approach. *Journal of Neurochemistry*, *85*(6), 1581–1591. https://doi.org/10.1046/j.1471-4159.2003.01818.x

Serrano-Pozo, A., Frosch, M. P., Masliah, E., & Hyman, B. T. (2011). Neuropathological Alterations in Alzheimer Disease. *Cold Spring Harbor Perspectives in Medicine*, *1*(1), a006189–a006189. https://doi.org/10.1101/cshperspect.a006189

Sevigny, J., Chiao, P., Bussière, T., Weinreb, P. H., Williams, L., Maier, M., … Sandrock, A. (2016). The antibody aducanumab reduces Aβ plaques in Alzheimer's disease. *Nature*, *537*(7618), 50–56. https://doi.org/10.1038/nature19323

Seyfried, N. T., Dammer, E. B., Swarup, V., Nandakumar, D., Duong, D. M., Yin, L., … Levey, A. I. (2017). A Multi-network Approach Identifies Protein-Specific Co-expression in Asymptomatic and Symptomatic Alzheimer's Disease. *Cell Systems*, *4*(1), 60-72.e1-e4. https://doi.org/10.1016/j.cels.2016.11.006

Sherrington, R., Froelich, S., Sorbi, S., Campion, D., Chi, H., Rogaeva, E., … St George-Hyslop, P. (1996). Alzheimer's disease associated with mutations in presenilin 2 is rare and variably penetrant. *Human Molecular Genetics*, *5*(7), 985–988. https://doi.org/10.1093/hmg/5.7.985

Smith, M. A., Kalaria, R. N., & Perry, G. (1993). α1-Trypsin Immunoreactivity in Alzheimer Disease. *Biochemical and Biophysical Research Communications*, *193*(2), 579–584. https://doi.org/10.1006/bbrc.1993.1663

Soltwisch, J., Kettling, H., Vens-Cappell, S., Wiegelmann, M., Muthing, J., & Dreisewerd, K. (2015). Mass spectrometry imaging with laser-induced postionization. *Science*, *348*(6231), 211–215. https://doi.org/10.1126/science.aaa1051

Stensballe, A., & Jensen, O. N. (2004). Phosphoric acid enhances the performance of Fe (III) affinity chromatography and matrix-assisted laser desorption / ionization tandem mass spectrometry for recovery , detection and sequencing of phosphopeptides. *Rapid Communications in Mass Spectrometry*, *18*(15), 1721–1730. https://doi.org/10.1002/rcm.1542

Stoeckli, M., Knochenmuss, R., McCombie, G., Mueller, D., Rohner, T., Staab, D., & Wiederhold, K. (2006). MALDI MS Imaging of Amyloid. In *Methods in enzymology* (Vol. 412, pp. 94–106). https://doi.org/10.1016/S0076-6879(06)12007-8

Stoeckli, M., Staab, D., Staufenbiel, M., Wiederhold, K., & Signor, L. (2002). Molecular imaging of amyloid β peptides in mouse brain sections using mass spectrometry. *Anal Biochem.*, *311*(1), 33–39. https://doi.org/10.1016/S0003-2697(02)00386-X

Strupat, K., Karas, M., & Hillenkamp, F. (1991). 2,5-Dihydroxybenzoic acid: a new matrix for laser desorption—ionization mass spectrometry. *International Journal of Mass Spectrometry and Ion Processes*, *111*, 89–102. https://doi.org/10.1016/0168-1176(91)85050-V

Sturchler-Pierrat, C., Abramowski, D., Duke, M., Wiederhold, K.-H., Mistl, C., Rothacher, S., … Sommer, B. (1997). Two amyloid precursor protein transgenic mouse models with Alzheimer disease-like pathology. *Proceedings of the National Academy of Sciences*, *94*(24), 13287–13292. https://doi.org/10.1073/pnas.94.24.13287

Sullivan, C., Berg, E., Elliott-Bryant, R., Fishman, J., McKee, A., Morin, P., … Fine, R. (2011). Pyroglutamate-Aβ 3 and 11 colocalize in amyloid plaques in Alzheimer's disease cerebral cortex with pyroglutamate-Aβ 11 forming the central core. *Neurosci Lett.*, *505*(2), 109–112. https://doi.org/10.1016/j.neulet.2011.09.071

Szklarczyk, D., Franceschini, A., Wyder, S., Forslund, K., Heller, D., Huerta-Cepas, J., … von Mering, C. (2015). STRING v10: protein–protein interaction

networks, integrated over the tree of life. *Nucleic Acids Research*, *43*(D1), D447–D452. https://doi.org/10.1093/nar/gku1003

Takeuchi, A., Irizarry, M. C., Duff, K., Saido, T. C., Hsiao Ashe, K., Hasegawa, M., … Iwatsubo, T. (2000). Age-Related Amyloid β Deposition in Transgenic Mice Overexpressing Both Alzheimer Mutant Presenilin 1 and Amyloid β Precursor Protein Swedish Mutant Is Not Associated with Global Neuronal Loss. *The American Journal of Pathology*, *157*(1), 331–339. https://doi.org/10.1016/S0002-9440(10)64544-0

Tanaka, K., Waki, H., Ido, Y., Akita, S., Yoshida, Y., Yoshida, T., & Matsuo, T. (1988). Protein and polymer analyses up tom/z 100 000 by laser ionization time-of-flight mass spectrometry. *Rapid Communications in Mass Spectrometry*, *2*(8), 151–153. https://doi.org/10.1002/rcm.1290020802

Tillberg, P. W., Chen, F., Piatkevich, K. D., Zhao, Y., Yu, C.-C., English, B. P., … Boyden, E. S. (2016). Protein-retention expansion microscopy of cells and tissues labeled using standard fluorescent proteins and antibodies. *Nature Biotechnology*, *34*(9), 987–992. https://doi.org/10.1038/nbt.3625

Ulrich, J. D., Finn, M., Wang, Y., Shen, A., Mahan, T. E., Jiang, H., … Holtzman, D. M. (2014). Altered microglial response to Aβ plaques in APPPS1-21 mice heterozygous for TREM2. *Molecular Neurodegeneration*, *9*(1), 9. https://doi.org/10.1186/1750-1326-9-20

van Dyck, C. H. (2018). Anti-Amyloid-β Monoclonal Antibodies for Alzheimer's Disease: Pitfalls and Promise. *Biological Psychiatry*, *83*(4), 311–319. https://doi.org/10.1016/j.biopsych.2017.08.010

Wilm, M. (2011). Principles of Electrospray Ionization. *Molecular & Cellular Proteomics*, *10*(7), M111.009407. https://doi.org/10.1074/mcp.M111.009407

Wong, S. F., Meng, C. K., & Fenn, J. B. (1988). Multiple charging in electrospray ionization of poly(ethylene glycols). *The Journal of Physical Chemistry*, *92*(2), 546–550. https://doi.org/10.1021/j100313a058

World Health Organization. (2017). Global action plan on the public health response to dementia 2017-2025, 52. ISBN: 978-92-4-151348-7. Retrieved from http://www.who.int/mental_health/neurology/dementia/action_plan_2017_2025/en/

Xiong, F., Ge, W., & Ma, C. (2019). Quantitative proteomics reveals distinct composition of amyloid plaques in Alzheimer's disease. *Alzheimer's & Dementia*, *15*(3), 429–440. https://doi.org/10.1016/j.jalz.2018.10.006

Xu, G., Ran, Y., Fromholt, S. E., Fu, C., Yachnis, A. T., Golde, T. E., & Borchelt, D. R. (2015). Murine Aβ over-production produces diffuse and compact Alzheimer-type amyloid deposits. *Acta Neuropathologica Communications*, *3*(1), 72. https://doi.org/10.1186/s40478-015-0252-9

Yamashita, M., & Fenn, J. B. (1984). Electrospray ion source. Another variation on the free-jet theme. *The Journal of Physical Chemistry*, *88*(20), 4451–4459. https://doi.org/10.1021/j150664a002

Yang, J., & Caprioli, R. M. (2011). Matrix Sublimation/Recrystallization for Imaging Proteins by Mass Spectrometry at High Spatial Resolution. *Analytical Chemistry.*, *83*(14), 5728–5734. https://doi.org/10.1021/ac200998a

Yeo, J. C., Wall, A. A., Luo, L., & Stow, J. L. (2016). Sequential recruitment of Rab GTPases during early stages of phagocytosis. *Cellular Logistics*, *6*(1), e1140615. https://doi.org/10.1080/21592799.2016.1140615

Zempel, H., & Mandelkow, E. (2014). Lost after translation: missorting of Tau protein and consequences for Alzheimer disease. *Trends in Neurosciences*, *37*(12), 721–732. https://doi.org/10.1016/j.tins.2014.08.004

Zhang, Y., & Lee, D. H. S. (2011). Sink Hypothesis and Therapeutic Strategies for Attenuating Aβ Levels. *The Neuroscientist*, *17*(2), 163–173. https://doi.org/10.1177/1073858410381532

Zotova, E., Holmes, C., Johnston, D., Neal, J. W., Nicoll, J. A. R., & Boche, D. (2011). Microglial alterations in human Alzheimer's disease following Aβ42 immunization. *Neuropathology and Applied Neurobiology*, *37*(5), 513–524. https://doi.org/10.1111/j.1365-2990.2010.01156.x

APPENDICES

[Page left blank intentionally]

Appendix A. Expansion microscopy

Tissue dissection, antigen retrieval and immunostaining

Animals were anesthetized with avertin (1ml/100 g) and transcardial perfused with KPBS containing heparin (two minutes; 12 ml/min flow) followed by 4% paraformaldehyde (PFA) (10 minutes; 12 ml/min flow). Brains were incubated overnight (O/N) in 4% PFA solution at 4°C, washed and stored in KPBS/0.01% sodium azide until further use. Brains were cryoprotected by immersing in 30% sucrose (w/v) in KPBS for two days on shake at 4°C prior to freezing with dry ice and sectioning 100 µm coronal sections on a cryostat (Leica CM3050 S). Sections were stored in 1.5 ml tubes containing KPBS/0.01% sodium azide at 4°C.

Antigen retrieval was performed by incubating tissue sections in 80% formic acid/ddH_2O for 15 minutes at room temperature (RT) followed by heat treatment (95°C) in an alkaline buffer for 10 minutes (100 mM Tris base, 5% (w/v) triton X-100, 1% sodium dodecyl sulfate (SDS) in water. Tissue sections were washed twice in 1XPBS (five minutes each, RT, shake) between and after the antigen retrieval. The tissue sections were permeabilized in blocking buffer (1XPBS, 1% bovine albumin serum (BSA), 0.3% triton X-100, 5% normal swine serum (NS)) for five hours at RT on shake. Mouse antibodies (1:100, mouse 6E10, BioLegend; 1:100, mouse MN1060, Invitrogen; 1:50, mouse sc-271384, Santa-Cruz; 1:100, mouse sc-48342, Santa-Cruz; 1:100, rabbit D54D2, Ambient; 1:400, rabbit GA524, DAKO; 1:100, goat Ab5076, Abcam) were tested for four days, followed by incubation with (1:200; αMouse, αGoat or αRabbit; all IgG (H+L) secondary antibodies conjugated with alexa flour 488, 555 or 647, respectively (Thermo Fisher) for six hours at RT on shake. Sections were incubated in washing buffer (1XPBS, 0.25% BSA, 0.1% triton X-100) 4 x 15 minutes in between and after antibody staining at RT on shake.

Gelation, digestion, expansion and mounting

The stained sections were incubated in acryloyl-X SE/anhydrous (AcX, Invitrogen, prepared in dimethyl sulfoxide (DMSO), Sigma) O/N at RT on shake, washed twice

in 1XPBS for 15 minutes and incubated in gelation solution (monomer solution, 0.01% w/v 4-Hydroxy-TEMPO (4-HT; Sigma), 0.2% v/v tetramethylethylenediamine (TEMED; Sigma), 0.2% w/v ammonium persulfate (APS; Sigma)) for two hours in humidified 37°C incubation chamber. Monomer solution was prepared by mixing 8.6% w/v sodium acrylate (Sigma), 2.5% w/v acrylamide (Sigma), 0.15% v/v N,N'-methylenebisacrylamide (Sigma), 11.7% w/v sodium chloride, 1XPBS. Tissue-gels were incubated O/N at RT in digestion buffer containing; 0.5% triton X-100, 0.2% ethylenediaminetetraacetic acid (EDTA) (0.5M, pH 8), 5% Tris HCl (1M, pH 8), 4.67 g NaCl, proteinase K (final conc. 8 U/ml; New England Biolabs). Tissue-gels were expanded by incubating in ddH_2O four times for 15 minutes. Imaging was conducted on an LSM 880 upright confocal setup (Zeiss).

ISSN (online): 2246-1302
ISBN (online): 978-87-7210-567-3

AALBORG UNIVERSITY PRESS